Genome-wide RNAi screen identifies novel players in human 60S subunit biogenesis including key enzymes of polyamine metabolism

Dörner, Kerstin

2022-03-21

Dörner , K , Badertscher , L , Horvath , B , Hollandi , R , Molnar , C , Fuhrer , T , Meier , R , Sarazova , M , van den Heuvel , J , Zamboni , N , Horvath , P & Kutay , U 2022 , ' Genome-wide RNAi screen identifies novel players in human 60S subunit biogenesis including key enzymes of polyamine metabolism ' , Nucleic Acids Research , vol. 50 , no. 5 , þÿ p p . 2872 2888 . h t t p s : / / d o i . o r g / 1 0 . 1 0 9 3 / n a r / g k a c 0 7 2

http://hdl.handle.net/10138/355848
https://doi.org/10.1093/nar/gkac072

2872–2888 *Nucleic Acids Research, 2022, Vol. 50, No. 5* *Published online 12 February 2022*
https://doi.org/10.1093/nar/gkac072

Genome-wide RNAi screen identifies novel players in human 60S subunit biogenesis including key enzymes of polyamine metabolism

Kerstin Dörner[1,2], Lukas Badertscher[1,2], Bianka Horváth[1,2], Réka Hollandi[3], Csaba Molnár[3], Tobias Fuhrer[4], Roger Meier[5], Marie Sárazová[1], Jasmin van den Heuvel[1], Nicola Zamboni[4], Peter Horvath[3,6] and Ulrike Kutay[1,*]

[1]Institute of Biochemistry, Department of Biology, ETH Zurich, 8093 Zurich, Switzerland, [2]Molecular Life Sciences Ph.D. Program, 8057 Zurich, Switzerland, [3]Synthetic and Systems Biology Unit, Biological Research Center, 6726 Szeged, Hungary, [4]Institute of Molecular Systems Biology, Department of Biology, ETH Zürich, 8093 Zürich, Switzerland, [5]ScopeM, ETH Zürich, 8093 Zürich, Switzerland and [6]Institute for Molecular Medicine Finland, University of Helsinki, 00014 Helsinki, Finland

Received November 25, 2021; Revised January 18, 2022; Editorial Decision January 19, 2022; Accepted January 25, 2022

ABSTRACT

Ribosome assembly is an essential process that is linked to human congenital diseases and tumorigenesis. While great progress has been made in deciphering mechanisms governing ribosome biogenesis in eukaryotes, an inventory of factors that support ribosome synthesis in human cells is still missing, in particular regarding the maturation of the large 60S subunit. Here, we performed a genome-wide RNAi screen using an imaging-based, single cell assay to unravel the cellular machinery promoting 60S subunit assembly in human cells. Our screen identified a group of 310 high confidence factors. These highlight the conservation of the process across eukaryotes and reveal the intricate connectivity of 60S subunit maturation with other key cellular processes, including splicing, translation, protein degradation, chromatin organization and transcription. Intriguingly, we also identified a cluster of hits comprising metabolic enzymes of the polyamine synthesis pathway. We demonstrate that polyamines, which have long been used as buffer additives to support ribosome assembly *in vitro*, are required for 60S maturation in living cells. Perturbation of polyamine metabolism results in early defects in 60S but not 40S subunit maturation. Collectively, our data reveal a novel function for polyamines in living cells and provide a rich source for future studies on ribosome synthesis.

INTRODUCTION

All known organisms rely on ribosomes for translating messenger RNAs (mRNAs) into proteins. Ribosomes are macromolecular complexes consisting of a large and a small subunit, each composed of ribosomal RNA (rRNA) and ribosomal proteins. Human 40S subunits are built of the 18S rRNA and 33 ribosomal proteins (RPSs), whereas 60S subunits harbor three rRNAs, 28S, 5.8S and 5S, as well as 47 ribosomal proteins (RPLs).

Early steps of ribosome maturation occur in the nucleolus, where RNA polymerase I transcribes a polycistronic pre-rRNA that contains the 18S, 5.8S and 28S rRNAs surrounded by external and internal transcribed spacer regions. The emerging pre-rRNA is quickly bound by early assembling ribosomal proteins as well as ribosome biogenesis factors (RBFs). These non-ribosomal proteins function as chaperones, processing and assembly factors, supporting rRNA modification, folding and compaction as well as incorporation of ribosomal proteins (1–5). During the assembly process, the three mature rRNAs are excised from the pre-rRNA by a series of endo- and exonucleolytic rRNA cleavage and trimming steps (6–9). A critical cleavage step occurs in the initially formed 90S particle to separate the emerging pre-40S and pre-60S particles. The released pre-40S particle progresses through several nucleoplasmic maturation events and is

*To whom correspondence should be addressed. Tel: +41 446323013; Email: ulrike.kutay@bc.biol.ethz.ch
Present addresses:
Lukas Badertscher, Aelian Biotechnology GmbH, 1030 Wien, Austria.
Csaba Molnár, Broad Institute of MIT and Harvard, Cambridge, MA 02142, USA.
Marie Sárazová, Institute for Evolution and Biodiversity, University of Münster, 48149 Münster, Germany.
Jasmin van den Heuvel, Celerion Switzerland AG, 8320 Fehraltorf, Switzerland.

then rapidly exported to the cytoplasm. Meanwhile the pre-60S particle undergoes extensive nucle(ol)ar remodeling before it reaches competence for nuclear export. These 60S maturation steps involve several ATPases and GTPases that catalyze energy-dependent reactions, directing the assembly process (1,10). Intertwined folding events of the six subdomains of the 28S rRNA first yield major parts of the solvent-exposed regions of the pre-60S particle. Internal structures of the 60S subunit including the catalytic peptidyl transferase center (PTC) and the peptide exit tunnel (PET) start forming during later nucleolar maturation steps. Besides 28S and 5.8S rRNA, 60S subunits also contain the 5S rRNA, transcribed by RNA polymerase III, which is incorporated into maturing pre-60S particles in nucleoli as a 5S RNP complex with RPL5/uL18 and RPL11/uL5. Both small and large subunits require a series of final biogenesis steps in the cytoplasm, giving rise to mature, translationally competent 40S and 60S subunits.

Illustrating the importance of ribosome synthesis for cellular growth and homeostasis, many regulatory pathways govern ribosome biogenesis, including extracellular signaling and internal stress response pathways that adjust the production of new ribosomes to cellular needs (11,12). An increase in size and number of nucleoli, which reflects enhanced ribosome production, has been known as a hallmark of cancer for more than a century (13). Increased ribosome production and changed ribosomal modifications have also been suggested to directly promote tumor development (11). Therefore, even though ribosome biogenesis is essential in both normal and malignant cells, it can serve as a target for cancer therapy (14). Importantly, impaired ribosome biogenesis can also manifest in a class of severe congenital conditions generally referred to as ribosomopathies (8,15,16). Defects in nucleolar steps of ribosome biogenesis can activate a nucleolar stress response pathway that is initiated by a failure to incorporate the 5S RNP into nascent 60S subunits. The 5S RNP then binds and inhibits the p53 E3 ubiquitin ligase MDM2/HDM2, leading to p53 stabilization and cell cycle arrest, eventually followed by apoptosis or senescence (8,17,18).

The highly orchestrated and complex process of ribosomal subunit assembly in eukaryotes involves more than 350 RBFs, which support pre-rRNA folding, modification and processing as well as the concomitant deposition of ribosomal proteins on the rRNAs (1,4,19). Besides RBFs, cells also rely on other cellular key processes for ribosome production, including transcription by all three RNA polymerases, splicing, mRNA processing as well as translation and nuclear transport. Most of the currently known eukaryotic RBFs were initially identified by studies in budding yeast exploiting genetic screens or affinity purification of pre-ribosomal particles followed by mass spectrometry (20–28). Biochemical and structural analyses of precursor particles then revealed the molecular function of a number of RBFs (1,4). Yet, although many principles of ribosome biogenesis are conserved from yeast to human, RNAi screens have revealed that synthesis of human ribosomes requires additional factors and unique regulatory mechanisms (29–33). Screens for human RBFs have so far focused on the function of nucleolar factors in rRNA processing, the regulation of nucleolar numbers and the identification of factors involved in 40S biogenesis (29–33). However, only selected candidates have been tested for a possible function in the maturation of the large ribosomal subunits until now.

To generate an unbiased inventory of factors required for human 60S assembly, we performed a genome-wide RNAi screen in human cells using the localization of RPL29/eL29-GFP as a readout. We screened two genome-wide libraries each targeting ∼20 000 genes with on average seven siRNAs per gene, and confirmed unexpected hits in a validation screen. In total, we identified 310 high confidence factors required for nucle(ol)ar steps of 60S maturation, including some major cellular protein modules contributing to subunit maturation. In addition, we found numerous factors that have hitherto not been linked to 60S subunit production, among them metabolic enzymes involved in polyamine synthesis. Our follow-up analysis indeed confirmed a requirement of polyamine metabolism specifically for efficient large subunit maturation, highlighting the validity and potency of our dataset.

MATERIALS AND METHODS

Reagents

For a complete list of reagents please refer to Supplementary Table S1.

Cell lines, drugs and antibodies

All cell lines were grown in DMEM supplemented with 10% fetal calf serum (FCS) and 100 μg/ml penicillin/streptomycin (DMEM+/+) at 37°C in 5% CO_2. The tetracycline-inducible HeLa RPS2-YFP and HeLa RPL29-GFP cells have been described previously (30,31). HeLa K cells were a kind gift from D. Gerlich (IMBA, Vienna, Austria). All cell lines tested negative for mycoplasma using PCR assays. HeLa RPL29-GFP cells were induced for 8 h by addition of 0.5 μg/ml tetracycline, followed by a 20 h chase period in tetracycline-free medium before fixation. HeLa RPS2-YFP cells were induced for 16 h, followed by a 4 h chase period in tetracycline-free medium before fixation.

Tetracycline (cat. no. 550205) and DL-α-difluoromethylornithine hydrochloride hydrate (DFMO, cat. no. D193) were purchased from Sigma-Aldrich, leptomycin B (LMB; cat. no. L-6100) from LC Laboratories, and cycloheximide (CHX; cat. no. C7698) from Invitrogen.

The following commercial antibodies were used in this study: anti-β-actin (Santa Cruz Biotechnology, sc-47778), anti-AMD1 (Proteintech, 11052–1-AP), anti-GFP (Santa Cruz Biotechnology, sc-9996), anti-HSP60 (Abcam, ab45134), anti-MRTO4 (Santa Cruz Biotechnology, sc-81856), anti-ODC1 (Abcam, ab193338), anti-RPL11 (uL5) (Abcam, ab79352), anti-RPS4X (eS4X) (Abcam, ab211427), anti-RPL29 (eL29) (Abcam, ab88514). Other used antibodies have been described previously: anti-RPL23A (uL23) (34), anti-RPS3 (uS3) (35), anti-LSG1 (36), anti-ENP1 (35), anti-RRP12 (34).

siRNA screening libraries

Two genome-wide siRNA libraries from Qiagen and Ambion/Thermo Fisher Scientific were used in this study. The custom-designed screening plates were produced at the ETH Zurich Scientific Center for Optical and Electron Microscopy (ScopeM). The Qiagen siRNA library consisted of three Qiagen libraries containing ∼four siRNAs per gene: HsDgV3 (druggable genome), HsNmV1 (genome extension) and HsXmV1(predicted genes). The library was re-annotated using an updated version of the human transcriptome and contained ∼72'000 siRNAs targeting ∼19 000 genes. The final Qiagen library contained 296 assay plates in a 384-well plate format. Control siRNAs were placed in columns 1, 2, 23 and 24 (Supplementary Figure S1C). As a second genome-wide library the Silencer Select Human Genome siRNA Library V4 was obtained from Ambion/Thermo Fisher Scientific. It contained ∼three siRNAs per gene, in total ∼59 000 siRNAs targeting roughly 20 500 genes. The Ambion screening library was pipetted on 192 assay plates in a 384-well plate format. Pre-tested control siRNAs were placed in columns 23 and 24 (Supplementary Figure S1C). A custom siPool library was purchased from siTOOLs Biotech for validation screening, with each pool being a mix of 30 individual siRNAs against the target gene. The library contained 480 siPools targeting high ranking genes of the genome-wide screens that had not previously been associated with ribosome biogenesis. Validation screening was performed using two 384 well plates per replicate, with pre-tested control siPools scattered on each plate (Supplementary Figure S1C).

siRNA screening procedure

Qiagen and Ambion libraries were screened in four and three batches, respectively, with each batch containing one siRNA per gene. The three replicates of the validation screen with two plates each were processed independently. For reverse transfection, DMEM was mixed with Lipofectamine RNAiMax (Invitrogen) (0.1 μl RNAiMax in 20 μl DMEM), added to the wells, and incubated for 45 min at room temperature. Then HeLa RPL29-GFP cells were seeded (900 cells/well in 50 μl DMEM +/+). 44 h after transfection, expression of RPL29-GFP was induced by addition of 0.5 μg/ml tetracycline for 8 h. Cells were then washed with DMEM and cultured in tetracycline-free DMEM +/+ for 20 h. Cells were fixed in medium by addition of 14.7% paraformaldehyde in PBS (15 μl, containing 5.6 μg/ml Hoechst). During validation screening, the medium was removed, and cells were fixed with 4% formaldehyde in PBS (60 μl, containing 1 μg/ml Hoechst). After 15 min fixation, cells were washed three times with 95 μl H_2O and then kept in H_2O/NaN_3. Plates were imaged on a Molecular Devices ImageXpress microscope equipped with a Thermo CRS plate loader. Per well, nine images (Hoechst and GFP) were acquired with a 10× Plan Fluor 0.3 objective. Laser-based autofocus was used at each site. In total, ∼3 415 000 images were acquired (296 × 384 wells, 192 × 384 wells and 3 × 2 × 384 wells; per well: nine images, two channels).

Image processing and phenotype classification

After signal intensities were rescaled and corrected for batch effects and uneven illumination (37), cell nuclei were identified based on the Hoechst signal. For the genome-wide screens, a server-based version of the CellProfiler program (38) with custom modifications was used to segment cells and extract their properties. The cytoplasm was approximated as a ring around the cell nucleus (width of roughly 6.5 μm). Nuclei and cytoplasm were used as masks to extract various cell features (e.g. intensity values, texture, morphological descriptors). For the validation screen images were segmented with nucleAIzer (39). Advanced Cell Classifier (ACC), a supervised machine learning tool, was used to classify cells based on their phenotypes (40). The following categories were distinguished: wild-type, hits (cells with ribosome biogenesis defects), mitotic cells, apoptotic cells, cells without GFP signal and incorrectly segmented cells. Cells were classified with multi-layer perceptron (MPL) using the Weka library in ACC.

Hit classification and evaluation

Cell number cut-offs were chosen based on the cell count in si-PLK1 and si-KIF11 control wells. Thresholds were set by adding three standard deviations to the mean cell number of these cell death controls, resulting in the following thresholds: 370 for the Qiagen library, 385 for the Ambion library, 200 for the validation screen. To combine results obtained with the individual siRNAs in the genome-wide screens (3–7 siRNAs per gene), the redundant siRNA activity (RSA) algorithm (41) implemented in the R package 'scsR' (Bioconductor, DOI: 10.18129/B9.bioc.scsR) was used. RSA scoring was performed for the combined results of the Qiagen and Ambion libraries but also individually for each library.

In the validation screen, hits of the genome-wide screens were tested that had not been implicated in ribosome biogenesis directly or indirectly based on previous literature, but had an RSA *P*-value ≤0.0075 for the combined genome-wide screening results (Supplementary Table S5). Genes without evidence of mRNA and/or protein expression in HeLa cells were excluded. Further, all genes with an average hit rate of >0.3, or at least two siRNAs scoring higher than 0.5 were included in the validation screen, as well as genes in the top 300 hits in the RSA ranked hits of the individually analyzed Qiagen and Ambion libraries. Finally, additional interesting hits in the top 850 RSA ranked genes were selected for validation after visual inspection. Targets were considered validated if the average hit rate of the three biological replicates of the validation screen was greater than the mean false-positive rate plus five standard deviations (>0.229). Based on the selection criteria of the validation screen, the final hit list contains all genes expressed in HeLa cells with a *P*-value ≤0.0075. Genes that were non-hits in the validation screen were removed. After visual inspection of validation screen images, genes with >10% of cells classified as incorrectly segmented, reflecting multinucleation and mitotic escape, were excluded from the final hit list as well.

For evaluation of clusters of genes in the final hit list, the STRING database version 11.5 (42) and Cytoscape version

3.8.2 (43) were used. Gene ontology (GO) term analysis was performed using the PANTHER online tool version 16.0 (44). Disease associations of the hit genes were evaluated using the DisGeNET database, version v7 (45).

RNA interference

HeLa cells were transfected with siRNAs using Lipofectamine RNAiMax (Invitrogen). siPools (si-AMD1, si-ODC1) were purchased from siTOOLs and containing 30 different siRNAs each. The following single siRNAs were used: Allstars siRNA (Qiagen) si-control, si-RPL11 (GGUGCGGGAGUAUGAGUUA), si-RPS4X (CAAGGUGAAUGAUACCAUU). si-AMD1, si-ODC1 and siRPL11 were used at a final concentration of 5 nM for 48 h. si-RPS4X was used at 2.5 nM for 48 h.

Metabolomics

After removal of growth medium with an aspirator, cell culture plates containing 10^6 cells were washed twice with PBS and subsequently twice with freshly prepared 75 mM ammonium carbonate buffer pH 7.4. Plates were snap-frozen in liquid N_2 and stored at −80°C until further processing. After thawing, cells were extracted twice with 400 μl pre-cooled (−20°C) extraction solvent, consisting of acetonitrile, methanol and milliQ water (40:40:20, vol%) for 10 min at −20°C. Extracts were pooled and collected in 1.5 ml Eppendorf tubes including scraped cells from the second extraction. Extracts were centrifuged at 4°C and 14 000 rpm for 2 min and cell-free supernatants were transferred to 1.5 ml Eppendorf tubes and stored at −20°C.

Prior to measurements, supernatants were dried in a speed-vac at room temperature, resuspended in 120 μl ddH_2O and centrifuged at 14 000 rpm at 4°C for 5 min. 40 μl of clean precipitate-free supernatant was transferred to 96-well microtiter plates for analysis. Five microliters of sample were injected on to a Acquity UPLC BEH C18 Column, 130 Å, 1.7 μm, 2.1 mm × 30 mm installed on a LC–MS/MS system composed of a Shimadzu Nexera XR LC System coupled to an AB Sciex QTRAP 5500 mass spectrometer. Flow rate was kept constant at 0.4 ml/min using mobile phases composed of 0.1% formic acid in water (A) and acetonitrile (B). The gradient was run at 30°C as follows: 0 min, 0%; 1 min, 0%; 5 min, 30%; 6 min 50%; 7 min, 50%; 8 min, 0% B with 5 min initial equilibration time. The mass spectrometer was operated in positive mode with multiple reaction monitoring (MRM) settings provided as Supplementary Table S2. Quantification was achieved by measuring pure amino acids and freshly prepared polyamine standards.

Sucrose gradient analysis

Cells were pre-treated with 100 μg/ml CHX at 37°C for 3 min before harvest. For polysome profiling, cells were lysed in 10 mM Tris pH 7.5, 100 mM KCl, 10 mM $MgCl_2$, 1% (w/v) TX-100, 100 μg/ml CHX, 1 mM DTT and protease inhibitors. After removal of cell debris by centrifugation (10 000 g, 3 min, 4°C) 1 mg of total protein was loaded onto a linear 15–45% sucrose gradient in 50 mM HEPES pH 7.5, 100 mM KCl, 10 mM $MgCl_2$. After centrifugation (210 min, 38 000 rpm, Beckman Coulter SW41 rotor, 4°C), gradients were analyzed at OD_{254} with a Foxy Jr. Gradient collector (ISCO).

For analysis by immunoblotting, cells were lysed in 50 mM HEPES pH 7.5, 100 mM KCl, 3 mM $MgCl_2$, 0.5% (w/v) NP-40, 50 μg/ml CHX, 1 mM DTT and protease inhibitors. After removal of cell debris by centrifugation (16 000 g, 5 min, 4°C), 600 μg total protein were loaded onto a linear 10–45% sucrose gradient in 50 mM HEPES pH 7.5, 100 mM KCl, 3 mM $MgCl_2$. After centrifugation (80 min, 55 000 rpm, Beckman Coulter TLS55 rotor, 4°C), proteins in collected fractions were precipitated with trichloroacetic acid (TCA) and analyzed by immunoblotting.

rRNA pulse labeling

Cells were starved in phosphate-free DMEM (Invitrogen, cat. no. 11971–02) supplemented with 10% dialyzed FCS for 1 h at 37°C and subsequently pulse-labeled in phosphate-free DMEM containing ^{33}P phosphoric acid (20 μC/ml) for 1 h at 37°C. Cells were briefly washed in DMEM −/− and kept in non-radioactive DMEM +/+ until harvest after a chase period of 240 min. Total RNA was extracted using the RNeasy mini kit (Qiagen) and 800 ng total RNA were separated on a 1.2% agarose-formaldehyde gel in 50 mM HEPES pH 7.8, 1 mM EDTA (75 V, 3.5 h). RNA was stained with GelRed (Biotium, cat. no. 41003). After washing the gel with 75 mM NaOH for 15 min, 0.5 M Tris pH 7.0, 1.5 M NaCl for 20 min and 10× SSC for 10 min, RNA was transferred onto a nylon membrane (Hybond-N^+; GE Healthcare) by capillary transfer. The membrane was analyzed by phosphor-imaging using a Typhoon FLA 900 imager (GE Healthcare). Signals were then analyzed using the Fiji Software.

Northern blot analysis

Total RNA was extracted from cells using the RNeasy mini kit (Qiagen). Northern blot analysis was performed as described previously (32). 1.5 μg of total RNA were separated on a 1.2% agarose–formaldehyde gel in 50 mM HEPES pH 7.8, 1 mM EDTA (75 V, 5 h). RNA was stained with GelRed (Biotium, cat. no. 41003). After washing the gel with 75 mM NaOH for 15 min, 0.5 M Tris pH 7.0, 1.5 M NaCl for 20 min and 10X SSC for 10 min, RNA was transferred onto a nylon membrane (Hybond-N^+; GE Healthcare) by capillary transfer. After the RNA was UV crosslinked, the membrane was prehybridized in 50% (v/v) formamide, 5× SSPE, 5× Denhardt's solution, 1% SDS, 200 μg/ml DNA (Roche, cat#11467140001) for 1 h at 65°C. rRNA precursors were hybridized with radioactively (^{32}P) labeled probes (5′ITS1: CCTCGCCCTCCGGGCT CCGTTAATGATC, ITS2 GCGCGACGGCGGACGA CACCGCGGCGTC) (46) for 1 h at 65°C and subsequent overnight incubation at 42°C. After three washes for 5 min with 2× SSC at 37°C, the membrane was analyzed by phosphor-imaging using a Typhoon FLA 900 imager (GE Healthcare). Signals were then analyzed using the Fiji Software.

Immunofluorescence analysis and confocal microscopy

Cells grown on coverslips were fixed with 4% paraformaldehyde in PBS for 15 min at room temperature. After permeabilization with 0.1% Triton X-100, 0.02% SDS in PBS for 5 min, cells were blocked by incubation with 2% BSA in PBS (BSA/PBS) for 30 min. Next, cells were incubated with primary antibody diluted in BSA/PBS for 1 h, washed three times for 5 min with BSA/PBS and then incubated with secondary antibody diluted in BSA/PBS for 30 min. After three 5 min washes with PBS, coverslips were mounted onto glass slides with Vectashield (Vector Laboratories) for confocal microscopy. Images were acquired using a Zeiss LSM780 or LSM880 microscope with a 63× 1.4 NA oil DIC Plan-Apochromat objective.

Immunoblot analysis

Samples in SDS sample buffer were separated on SDS-PAGE gels and proteins were transferred to a nitrocellulose membrane by semi-dry blotting. After blocking the membrane with 4% milk in PBST for 30 min, it was incubated with primary antibody diluted in 4% milk in PBST over night at 4°C. The membrane was washed three times for 5 min with PBST and subsequently incubated with secondary antibody in 4% milk in PBST. After three further 5 min washes with PBST, the signal was either detected using a Fusion (Vilber) or an Odyssey (LI-COR) imaging system.

RESULTS

High-content screening identifies 310 factors required for 60S subunit maturation

To identify factors required for 60S ribosomal subunit maturation in human cells, we screened with two genome-wide siRNA libraries containing ∼72'000 siRNAs (∼four individual siRNAs per gene, Qiagen) and ∼59'000 siRNAs (∼three individual siRNAs per gene, Ambion), respectively (Figure 1A). The genome-wide libraries together targeted ∼20'500 genes with a coverage of 3–7 siRNAs per gene. As a readout for 60S maturation, we used a previously described ribosomal protein reporter, RPL29/eL29-GFP, expressed under control of a tetracycline-inducible promoter in HeLa cells (30). 44 h after reverse siRNA transfection, expression of RPL29-GFP was induced for 8 h followed by a 20 h chase period before fixation and automated fluorescence microscopy (Figure 1B).

Upon induction, RPL29-GFP is imported into the nucleolus, where it is incorporated into maturing ribosomal 60S subunits. RPL29-GFP containing ribosomes are then exported to the cytoplasm where they engage in translation, evidenced by the co-sedimentation of RPL29-GFP with polysome-containing fractions in a sucrose gradient (Supplementary Figure S1A). Interestingly, cells compensated for RPL29-GFP expression by lowering the level of endogenous RPL29 (Supplementary Figure S1B). In control cells, RPL29-GFP was mainly localized to the cytoplasm and nucleoli (Figure 1C, D). Perturbations of nucle(ol)ar steps of ribosome biogenesis, e.g. depletion of the ribosomal protein RPL11 or the pre-60S export factor XPO1/CRM1 (47,48), led to an accumulation of the reporter in nucleoli and the nucleoplasm (Figure 1D), which we used as a single-cell readout in the screening assay. As a negative control to determine the false-positive hit rate, we used a scrambled siRNA (si-control). In addition, we exploited cell death-inducing siRNAs targeting PLK1 and KIF11, which are commonly used to score for the efficiency of siRNA transfections (49–51), and to define a cell number threshold (Supplementary Figure S1C). In all three screens, we applied further positive controls targeting ribosomal proteins, RBFs and the nuclear transport machinery (Supplementary Figure S1C).

Image analysis was performed using an automated pipeline supporting illumination-correction (37), image segmentation based on Hoechst staining of cell nuclei and extraction of >150 features per cell. Next, we used the supervised machine learning software Advanced Cell Classifier (40) for phenotypic hit classification. The resulting hit rate describes the fraction of cells displaying nuclear accumulation of the RPL29-GFP reporter over all reporter-positive cells excluding mitotic or apoptotic cells (Supplementary Tables S3 and S4). To eliminate siRNAs with a strong negative effect on cell proliferation, we defined a cell number cut-off (Supplementary Figure S2D). We also excluded some genes that are not expressed in HeLa cells according to published transcriptomic and proteomic data (52,53). Based on the hit rates of all remaining siRNAs, we generated a preliminary ranked hit list by calculating the *P*-values for each gene using the redundant siRNA activity (RSA) algorithm (41) (Supplementary Table S5).

To validate selected high scoring hits not previously associated with ribosome biogenesis, we subsequently performed a validation screen in biological triplicates using pools of 30 siRNAs per gene (Supplementary Table S6). Because the individual siRNAs of the pools acted at a concentration of only 100 pM, off-target effects are known to be greatly reduced (54). Of the 480 genes tested in the validation screen, 83 could be validated using a very stringent cut-off that was defined as the mean hit rate of the negative control plus five standard deviations (Supplementary Table S7). In addition to these 83 validated hits, the final hit list contains 224 factors, which were previously shown to be involved in ribosome assembly and had a RSA-ranked *P*-value ≤0.0075 in the preliminary genome-wide hit list (Supplementary Table S8). Overall, this procedure identified 310 high confidence hit genes required for 60S maturation in human cells.

The robustness and reproducibility of the three screening campaigns were assessed using the control siRNAs present on all screening plates (Supplementary Figure S1C). Both genome-wide screens and the validation screen had high *Z'* scores (0.91, 0.9 and 0.84 for si-RPL11 against si-control in the Qiagen, Ambion and validation screens, respectively) reflecting the excellent separation of positive and negative control siRNAs as a numeric quality measure (Figure 1E). The hit rates and cell numbers of control siRNAs were comparable between screening batches/replicates (Supplementary Figure S2A–C). Moreover, the overall distribution of cell number and hit rates was similar for the two genome-wide screening libraries (Supplementary Figure S2D, E). Altogether, these data demonstrate

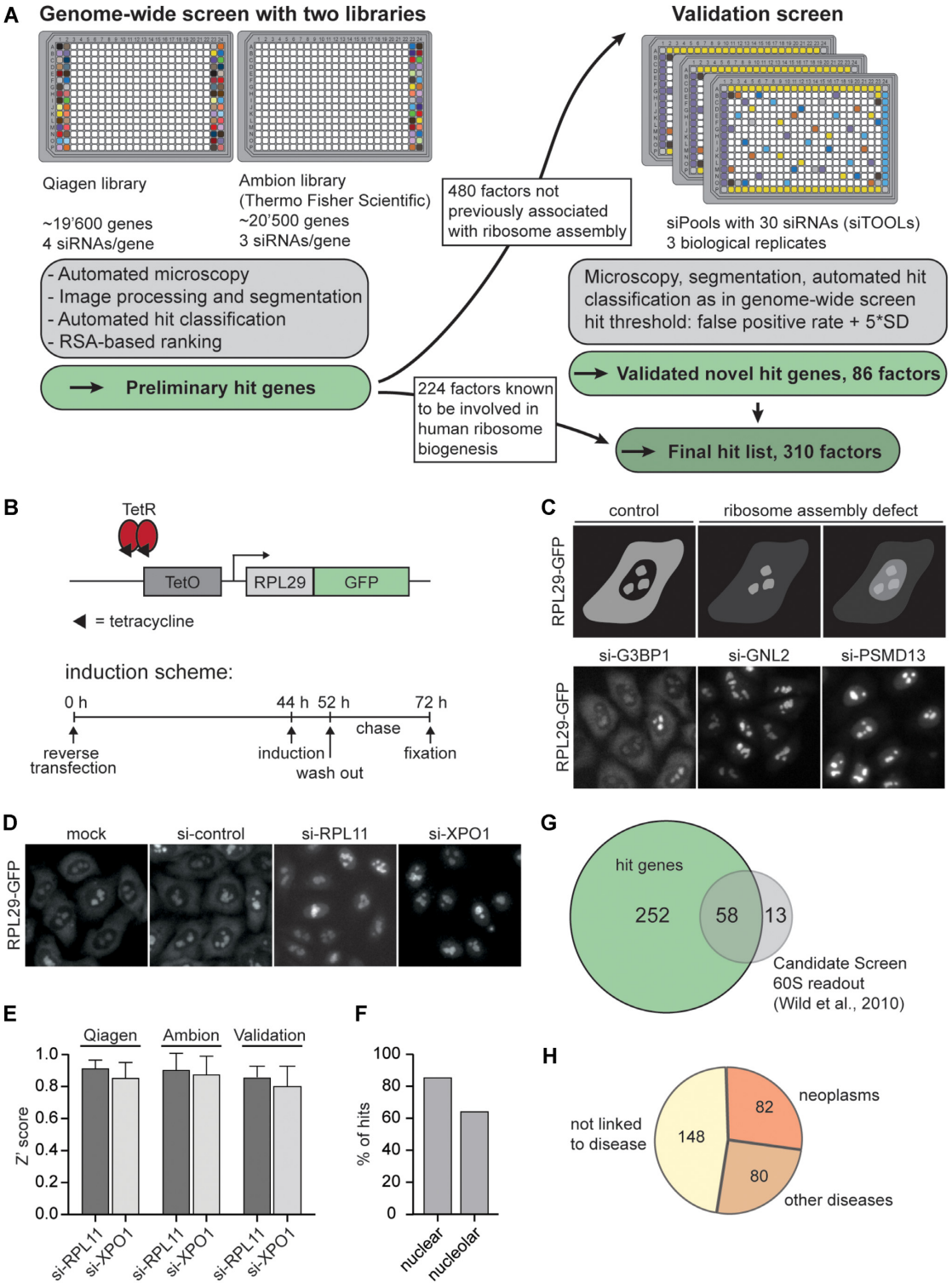

Figure 1. Genome-wide RNAi screen identifies factors required for 60S ribosomal subunit biogenesis. (**A**) Schematic overview of the screening campaign. We screened tetracycline-inducible HeLa RPL29-GFP cells with two genome-wide siRNA libraries with a total of ∼7 siRNAs per gene. Low confidence hits not previously implicated in ribosome biogenesis were validated using complex siPools, screening in biological triplicates. (**B**) Assay timeline. 44 h after reverse siRNA transfection, expression of RPL29-GFP was induced with tetracycline for 8 h, followed by a 20 h chase period in tetracycline-free medium. (**C**) Wild-type phenotype as well as defective ribosome biogenesis (hit) phenotypes of HeLa RPL29-GFP reporter cells with images of selected target siRNAs from the genome-wide screen. (**D**) Representative images of selected control siRNAs from the genome wide screen. (**E**) *Z'* scores for the positive control siRNAs RPL11/uL5 and XPO1 against negative control siRNA. (**F**) Percentage of final hits assigned to have a nuclear and nucleolar localization based on the Human Protein Atlas and the nucleolar proteome database (56), respectively. (**G**) Venn diagram showing the intersection of the 310 hits and the 71 large subunit biogenesis factors previously identified in a candidate screen using the same RPL29-GFP readout (31). (**H**) Venn diagram showing the number of hit genes associated with neoplasms or other diseases according to the DisGeNET database (45), (Supplementary Table S10).

the robustness of our RPL29-GFP-based screening campaigns.

More than 80% of the 310 high confidence hits are known to reside in the nucleus according to the Human Protein Atlas (55) (Figure 1F) and roughly 60% are found in nucleoli based on comparison with the Human Protein Atlas and the Nucleolar Proteome Database (NOPdb) (56–58). Nucle(ol)ar proteins were expected to be highly represented, since nucleoli are the cellular hub for ribosome production. In addition, we observed an excellent overlap (81.7%) with the hits of a previous candidate RNAi screen using the same reporter (31) (Figure 1G). Highlighting the organismal importance of ribosome synthesis, about half the hit genes (52%) are associated with diseases, particularly neoplasms, based on the DisGeNET database (45) (Figure 1H, Supplementary Table S10).

Several functional protein clusters support 60S subunit maturation

Gene ontology (GO) term overrepresentation analysis (59) revealed prominent GO-terms linked to ribosome biogenesis in all three categories, i.e. 'ribonucleoprotein complex biogenesis' and 'RNA processing' in the 'biological process' category, 'RNA binding' in the 'molecular function' category, and 'ribonucleoprotein complex' and 'ribosome' in the 'cellular component' category (Figure 2A). This illustrates that the hit list of the genome-wide 60S screen is highly enriched in proteins with known links to ribosome biogenesis and related cellular processes.

Next, we clustered the 310 hit genes based on high confidence protein–protein interactions annotated in the STRING database (42) and published literature, into twelve functional and one miscellaneous cluster (Figure 2B, Supplementary Table S9). Ribosomal proteins, in particular those of the large subunit, were highly enriched among the top-ranking hits. Almost all proteins of the 60S and approximately half of the proteins of the 40S subunit were scored as hits in the screen. Also, several known 60S-specific RBFs and factors involved in both 40S and 60S maturation were found as high- confidence hits, validating the screening approach. This genome-wide screen thus underlines the functional conservation of many 60S RBFs from yeast to humans, confirming previous candidate screens (31,32). Moreover, our data show for the first time that RLP24/RSL24D1 and DDX18, the human homologs of the yeast 60S biogenesis factors Rlp24 and Has1 respectively, function in human 60S subunit synthesis, in analogy to the yeast data (60,61). Interestingly, a few factors involved in early nucleolar steps of 40S biogenesis, including almost all members of the UTP-A complex, were also required for 60S biogenesis, reflecting the role of the UTP-A complex in the transcription of the joint pre-rRNA for both subunits (62,63).

An additional cluster of hits comprises proteins active in transcription, mRNA processing and chromatin remodeling. We identified subunits of all three RNA polymerases reflecting the requirement of rRNA, mRNA and snoRNA transcription for ribosome maturation. This is further echoed by other hits like DHX33 or TCOF1, which are involved in RNA polymerase I transcription (64,65), or BDP1, which is required for initiation of transcription by RNA polymerase III (66). Several members of the RNA polymerase II transcription initiation and elongation machinery are also part of the identified protein module. Moreover, the master transcriptional regulator MYC, which directly supports ribosome biogenesis (67), is a hit present in this cluster. We further identified several transcription and chromatin remodeling factors not previously implicated in human ribosome biogenesis. One example is FOXN1, one of several orthologs of the yeast transcription factor Fhl1, which is involved in ribosomal protein gene transcription in yeast (68,69). We also found KAT5, TRRAP and EP400, key components of the NuA4 complex as well as SET1A and WDR82, which are members of COMPASS complex. Both complexes function in chromatin remodeling, with the NuA4 complex acting as a histone acetyltransferase (70,71) and the COMPASS complex methylating H3K4 (72,73).

Notably, another cluster is formed by three members of the PP1 phosphatase complex, namely the catalytic PP1β subunit as well as the nuclear regulatory subunits PPP1R7 and PPP1R10. PP1 phosphatases have been linked to a variety of cellular processes, ranging from cell cycle control and metabolism to apoptosis (74). So far, only PP1γ was shown to interact with pre-60S subunits in human cells (75), and the role of these newly identified players remains to be investigated.

Other prominent clusters include the splicing, nuclear export, and translation machineries as well as the CCT complex, which aids folding of newly synthesized proteins. In addition, similar to our previous screening campaign on 40S subunit maturation (30), almost all proteasomal subunits were identified. Also, various other factors linked to protein ubiquitination scored highly, including several cullin-RING ubiquitin ligase components such as RBX1, DDB1, VPRBP, DCAF4L1, KCTD2 and ZER1 as well as all members of the COP9 signalosome. Some of these factors are also required for 40S biogenesis (30), but how they support ribosome synthesis is only poorly understood. Notably, VPRBP, a substrate adaptor for the CRL4 E3 ligase, has recently been linked to the degradation of the 60S subunit RBF PWP1 (76). Finally, the screen also revealed a number of uncharacterized factors such as ZSCAN23, UBAP2 and UBALD1, whose mechanistic roles remain to be explored. Taken together, these screening results provide a rich source of information to inform and guide future mechanistic studies as to how their action is linked to ribosome synthesis.

Key enzymes of the polyamine biosynthesis pathway are required for efficient 60S subunit synthesis

We were especially intrigued by a small cluster of hits comprising factors involved in metabolism. These three hits are functionally linked as they play an important role in cellular polyamine metabolism, namely AMD1, ODC1 and AZIN1 (Figure 3A). Polyamines are highly abundant, small and positively charged molecules. These polycations interact with negatively charged factors such as RNA,

Figure 2. Functional clusters of identified human factors contributing to 60S ribosomal subunit maturation. (**A**) Gene ontology (GO term) analysis for the final 310 hits by overrepresentation tests with respect to 'biological process', 'molecular function' and 'cellular component'. (**B**) Classification of the final 310 hits into functional clusters. Connections between genes represent high-confidence interactions reported by the STING database (interaction source: experiments, >0.7) (42).

DNA, ATP, but also proteins or lipids in various cellular processes (77,78). The adenosyl methionine decarboxylase AMD1 (hit list rank #88) and the ornithine decarboxylase ODC1 (hit list rank #108) are the rate-limiting enzymes of the polyamine synthesis pathway, which converts ornithine in a stepwise manner into putrescine, spermidine, and spermine (Figure 3A) (78–80). Specifically, ODC1 converts ornithine into the spermidine precursor putrescine, and AMD1 produces decarboxylated adenosyl-methionine, which is used in two consecutive steps to elongate putrescine into spermidine and then spermine. Other enzymes of the pathway did not rank among the top hits of the genome-wide screen (Figure 3B), but depletion of the regulatory factor AZIN1 (antizyme inhibitor 1, hit list rank #194)

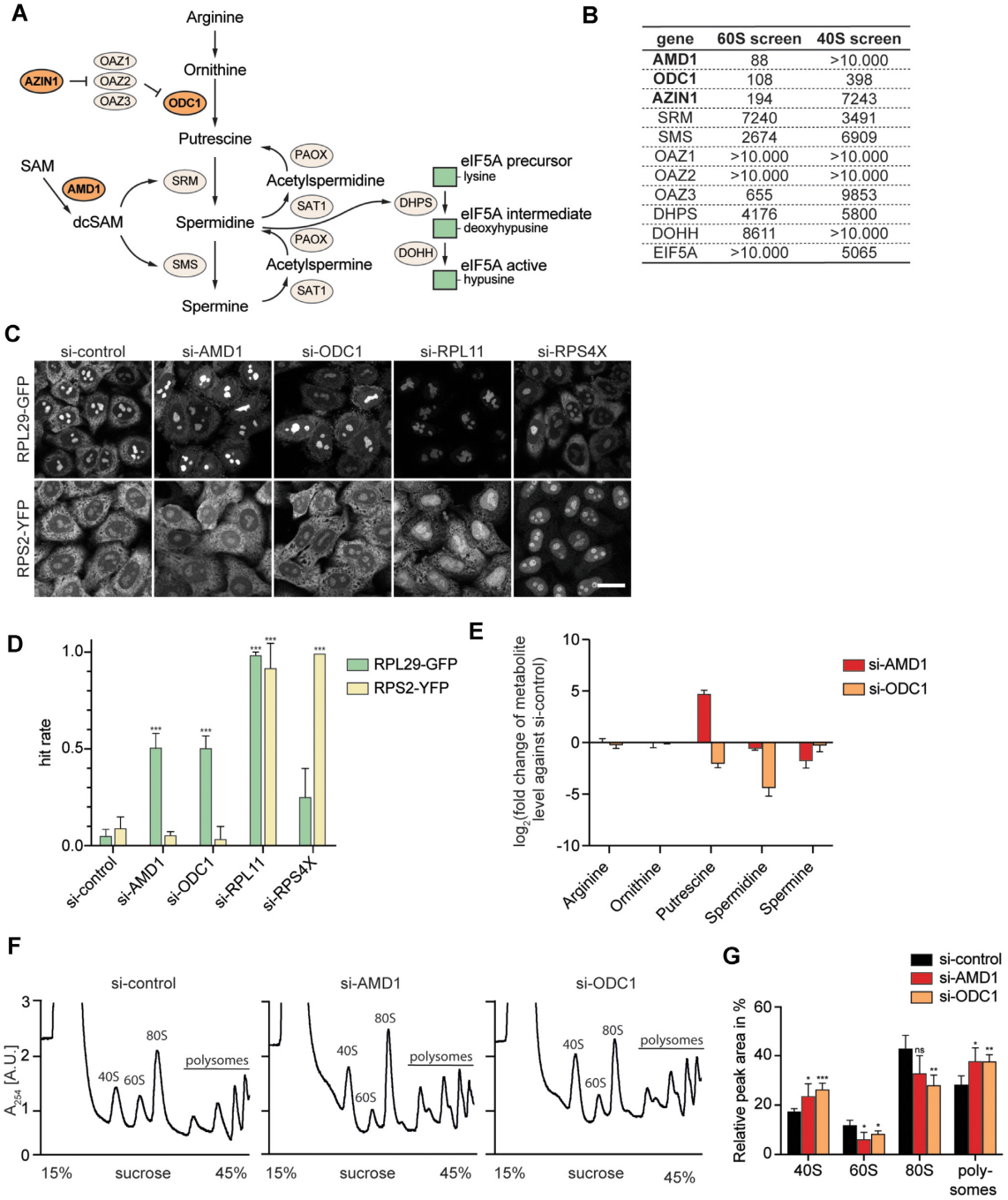

gene	60S screen	40S screen
AMD1	88	>10.000
ODC1	108	398
AZIN1	194	7243
SRM	7240	3491
SMS	2674	6909
OAZ1	>10.000	>10.000
OAZ2	>10.000	>10.000
OAZ3	655	9853
DHPS	4176	5800
DOHH	8611	>10.000
EIF5A	>10.000	5065

Figure 3. AMD1 and ODC1, rate-limiting enzymes of the polyamine metabolism, are required for 60S but not 40S subunit maturation. (**A**) Schematic representation of polyamine pathway including eIF5A hypusination. Hits in the 60S screen are highlighted in orange. (**B**) Ranks of polyamine synthesis pathway genes in the 60S screen and the previous 40S screen (30). Hits in the 60S screen are marked in bold. (**C**) Ribosomal reporter HeLa cell lines inducibly expressing RPL29-GFP or RPS2-YFP were depleted of the indicated proteins by RNAi (48 h). Expression of RPL29-GFP was induced for 8 h with tetracycline and chased in tetracycline-free medium for 20 h prior to fixation. Expression of RPS2-YFP was induced for 16 h, followed by a 4 h chase period. Scale bar: 20 μm. (**D**) Quantification of the fraction of cells with ribosome biogenesis defects (hit rate) in (C). Mean + SEM, $N = 3$, $n \geq 100$, unpaired *t*-test against si-control of the respective cell line, $^{***}P \leq 0.001$. (**E**) Levels of metabolites of the polyamine pathway upon RNAi-mediated depletion of AMD1 and ODC1 in HeLa K cells expressed as fold change relative to si-control. Mean + SEM. $N = 3$. (**F**) For polysome profiling, HeLa K cells were treated with the indicated siRNAs, followed by sucrose gradient centrifugation (15–45% sucrose) of cell extracts and recording the absorption at 254 nm along the gradient. (**G**) Quantification of four biological replicates of polysome profiles as shown in (F) determining the relative areas beneath the A254 peaks of 40S, 60S, 80S, and the first three polysome peaks. Mean ± SEM, $N = 4$, unpaired *t*-test against si-control, $^{*}P \leq 0.05$, $^{**}P \leq 0.01$, $^{***}P \leq 0.001$, ns = non-significant.

also resulted in significant 60S biogenesis defects. AZIN1 is a known positive regulator of ODC1, whose function is tightly regulated also at the post-transcriptional level. ODC1 needs to form a homodimer to be active but inhibitory proteins called antizymes (OAZ1, OAZ2, OAZ3) bind ODC1 monomers and promote their proteasomal degradation (81). AZIN1, which is structurally similar to ODC1, binds these antizymes with high affinity, thereby stabilizing ODC1 and promoting polyamine synthesis (82–84). Polyamines have been used for decades as buffer additives to stabilize isolated ribosomes, enhance *in vitro* translation efficiency and support *in vitro* reconstitution of ribosomal particles (85–88). In the 1980s, polyamines were implicated in rRNA synthesis in *E. coli* and human lymphocytes (89,90). Yet, these results were never followed up upon and a thorough investigation of the links between polyamine metabolism and ribosome biogenesis is missing.

To validate the screening results, ODC1 and AMD1 were depleted in HeLa RPL29-GFP reporter cells and in a previously described HeLa cell line inducibly expressing RPS2-YFP as a 40S subunit biogenesis reporter (31). While depletion of ODC1 or AMD1 resulted in 60S biogenesis defects, indicated by the accumulation of RPL29-GFP in nucleoli, RPS2-YFP localization remained unchanged (Figure 3C, D, Supplementary Figure S3A). This suggests that the lack of polyamines predominantly impairs 60S subunit maturation. To examine the impact of the RNAi-induced perturbations on polyamine metabolism, we analyzed cells depleted of AMD1 and ODC1 by targeted metabolomics. Depletion of both AMD1 or ODC1 indeed led to a reduction of spermine and spermidine levels compared to control conditions, while putrescine levels were affected differentially by the two treatments, in line with the distinct functions of AMD1 and ODC1 in the metabolic pathway (Figure 3A, E). Taken together, metabolomic analysis indicates that AMD1 or ODC1 depletion-mediated reduction in levels of the polyamines spermine and spermidine evokes 60S biogenesis defects.

To confirm these results, we next monitored the effects of AMD1 or ODC1 depletion on the dynamic shuttling behavior of ENP1, a 40S biogenesis factor (91,92), and RRP12, a factor involved in both 40S and 60S maturation (93) (Supplementary Figure S3B). Both ENP1 and RRP12 are enriched in nucleoli at steady state but accompany ribosomal subunits into the cytoplasm (35,93). Depletion of neither AMD1 nor ODC1 altered the steady state localization of ENP1 or RRP12. However, when we additionally inhibited nuclear export of ribosomal subunits by leptomycin B (LMB) treatment (47,48), RRP12 was retained in nucleoli while localisation of ENP1 was largely unchanged (Supplementary Figure S3B). This result supports a function of polyamines in early steps of 60S but not 40S biogenesis.

To investigate whether perturbations in polyamine metabolism affect ribosomal subunit stoichiometry or mRNA translation, we performed polysome profile analysis of Hela K cells depleted of AMD1 and ODC1. Indeed, AMD1 and ODC1 depletion resulted in smaller-sized 60S peaks concomitant with an increase in free 40S subunits and increased appearance of half-mer polysomes, indicating a shortage of 60S subunits (Figure 3F, G). Taken together, these data confirm the results obtained with the reporter cell lines and suggest that perturbation of polyamine metabolism strongly affects nuclear maturation of 60S but not 40S subunits.

AMD1 and ODC1 depletions result in defective rRNA processing

Next, we tested whether changes in polyamine metabolism influence rRNA maturation. In human cells, the 18S, 5.8S and 28S rRNAs are synthesized as parts of a polycistronic 47S rRNA precursor that undergoes a series of endo- and exonucleolytic processing reactions with several defined pre-rRNA intermediates to finally yield the three mature rRNAs (Figure 4A). We first investigated the effect of AMD1 and ODC1 depletion on pre-rRNA processing by radioactive ^{33}P pulse-labeling experiments. Hela K cells were analyzed after a 4 h period, during which cells processed the initially transcribed ^{33}P-labeled 47S pre-rRNA (Figure 4B). Perturbation of the polyamine synthesis pathway significantly reduced 28S rRNA production, while generation of 18S rRNA was only mildly affected. This was further underlined by the decreased ratio of 28S to 18S rRNA (Figure 4C). Consistent with these results, the analysis of total RNA by Northern blot with a probe against the ITS2 region revealed an accumulation of the 41S, 32S and 12S pre-rRNAs upon AMD1 or ODC1 depletion (Figure 4D, E). Accumulation of these precursors indicated defects in rRNA cleavage at sites 2 and 4 as well as defects in trimming of the 5.8S rRNA 3′end. Using a probe detecting 18S rRNA processing intermediates by targeting the ITS1 region, stabilisation of the 41S and a decrease of the 30S pre-rRNAs were observed, while later intermediates of the 18S maturation pathway were unchanged upon AMD1 or ODC1 depletion. Despite the mild accumulation of the 41S pre-rRNA, this did not manifest in an obvious 40S subunit biogenesis defect judged based on the RPS2-YFP reporter and the ENP1 readout (Figure 3C, Supplementary Figure S3B). Co-depletion of AMD1 and ODC1 did not result in significantly stronger effects on rRNA processing in pulse labeling or Northern blot analysis as expected given their function in the same pathway (Figure 4B–E). Together, analysis of rRNA processing revealed that depletion of AMD1 and ODC1 impinges in particular on the maturation of the 28S and 5.8S rRNAs.

Chemical inhibition of ODC1 leads to 60S biogenesis defects

To validate the RNAi-based experiments by an independent method, we manipulated cellular polyamine synthesis using a well-established chemical compound, difluoromethylornithine (DFMO), which inhibits the enzymatic activity of ODC1 (94–97). Metabolomic analysis showed that inhibition of ODC1 by DFMO results in similar albeit more pronounced changes in metabolite levels along the polyamine pathway compared to RNAi-mediated depletion of ODC1 (Figures 3E and 5A). Levels of spermidine and putrescine were strongly reduced, while spermine levels were only slightly decreased, as previously observed (98,99). In agreement with the RNAi depletion

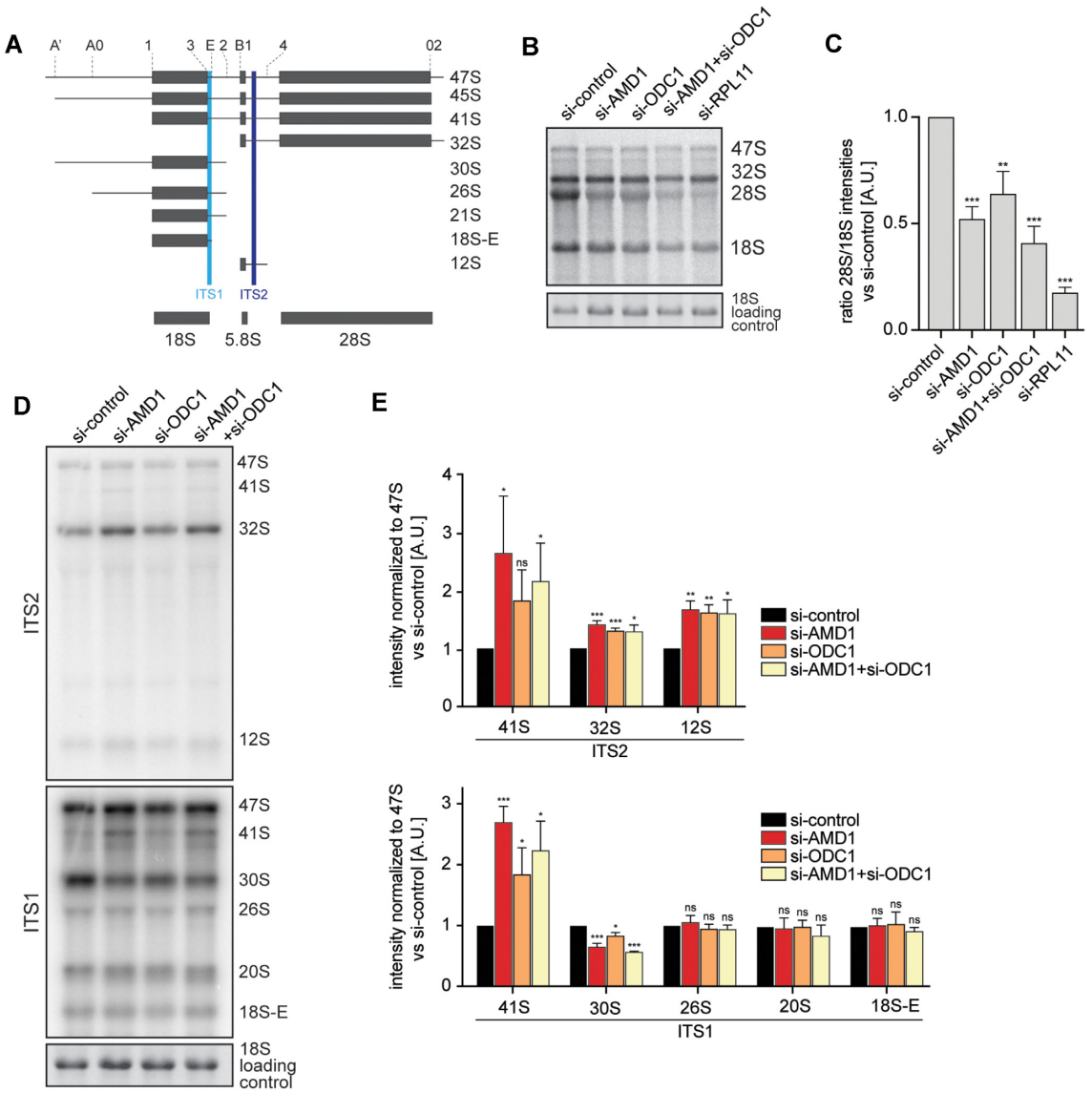

Figure 4. Depletion of AMD1 and ODC1 results in rRNA processing defects. (**A**) Illustration of major rRNA processing intermediates in human cells. rRNA regions bound by probes used for Northern blot experiments are indicated. (**B**) Hela K cells were treated with the indicated siRNAs and analyzed by pulse labeling with ^{33}P orthophosphate. Total RNA was extracted from cells harvested 240 min after ^{33}P washout. rRNA processing was analyzed by autoradiography. Levels of mature 18S rRNA were visualized with GelRed as loading control. (**C**) Quantification of the 28S/18S ratio of the autoradiograph in (B) expressed as fold change against si-control. Mean + SEM, $N = 3$, unpaired t-test against si-control, $^{**}P \leq 0.01$, $^{***}P \leq 0.001$. (**D**) Northern blot analysis of total RNA extracted from HeLa K cells treated with the indicated siRNAs using radioactively labelled probes targeting the ITS2 or ITS1 regions as indicated in (A). Levels of mature 18S rRNA were visualized with GelRed as a loading control. (**E**) Quantification of indicated rRNA precursors detected with the ITS2 or ITS1 probe shown in (D) normalized to the amount of 47S rRNA precursor and expressed as fold change relative to si-control. Mean + SEM, $N = 3$, unpaired t-test against si-control, $^{*}P \leq 0.05$, $^{**}P \leq 0.01$, $^{***}P \leq 0.001$, ns = non-significant.

experiments, DFMO treatment of the reporter cell lines revealed the accumulation of RPL29-GFP in nucleoli and the nucleoplasm, while the localization of RPS2-YFP was comparable to solvent-treated cells (Figure 5B, C). Effects of DFMO treatment on the localization of ENP1 and RRP12 also mirrored the results obtained by RNAi-mediated depletion of AMD1 and ODC1 (Supplementary Figure S4A). Specifically, the 60S and 40S biogenesis factor RRP12 was retained in nucleoli when cells were treated with DFMO and nuclear export of ribosomal subunits was blocked by LMB. Localization of the 40S biogenesis factor ENP1 on the other hand remained unchanged upon ODC1 inhibition by DFMO, in presence or absence of LMB. Together, these data reveal that ODC1 activity is required for nucle(ol)ar 60S maturation.

Next, we analyzed pre-rRNA processing in cells treated with DFMO or solvent by both the ^{33}P pulse labeling approach and Northern blot analysis. Pulse labeling experiments revealed a reduction of 28S production and a decreased 28S/18S ratio upon DFMO treatment (Supplementary Figure S4B, C), reflecting defects in 60S subunit maturation. A slight reduction in 18S rRNA production was also detected upon ODC1 inhibition, yet no defects in 40S subunit maturation were observed with

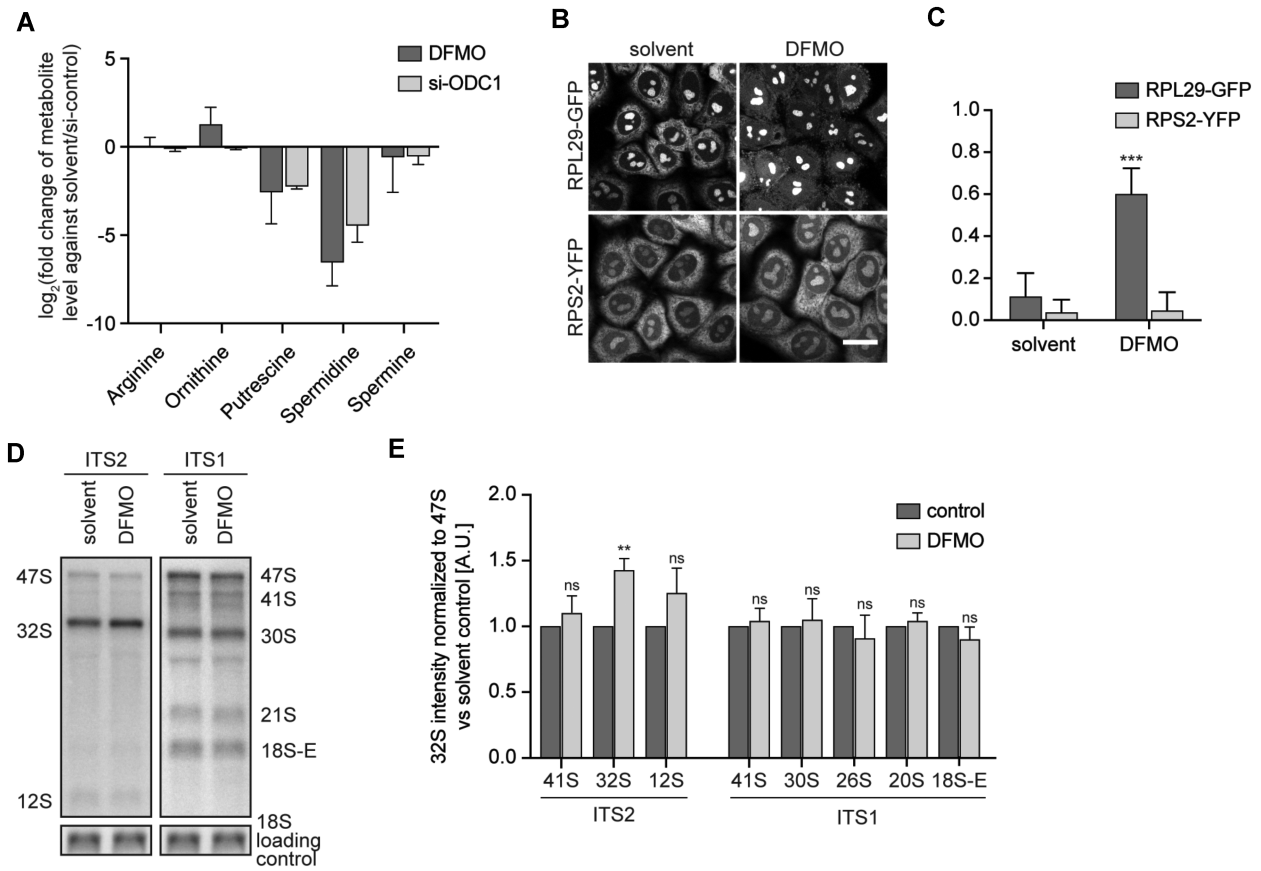

Figure 5. Inhibition of ODC1 with DFMO leads to defects in 60S subunit maturation. (**A**) Levels of metabolites of the polyamine pathway in HeLa K cells upon ODC1 inhibition with DFMO (2.5 mM, 48 h) expressed as fold change relative to solvent control. Mean + SEM, $N = 3$. Measurements of cells treated with si-ODC1 (Figure 3E) are shown for comparison. (**B**) Ribosomal reporter HeLa cell lines inducibly expressing RPL29-GFP or RPS2-YFP were treated with 2.5 mM DFMO or solvent control for 48 h. Expression of RPL29-GFP was induced for 8 h with tetracycline and chased in tetracycline-free medium for 20 h prior to fixation. Expression of RPS2-YFP was induced for 16 h, followed by a 4 h chase period. Scale bar: 20 μm. (**C**) Quantification of cells with ribosome biogenesis defects (hit rate) in (B). Mean + SEM, $N = 4$, $n \geq 160$, unpaired t-test against solvent control of the same cell line, $^{**}P \leq 0.01$. (**D**) Northern blot analysis of total RNA extracted from HeLa K cells treated with DFMO (2.5 mM, 48 h) or solvent control using radioactively labelled probes targeting the ITS2 or ITS1 region. Levels of mature 18S rRNA were visualized with GelRed as a loading control. (**E**) Quantification of rRNA precursors detected with ITS2 and ITS1 probes as shown in (D) normalized to the amount of 47S rRNA precursor and expressed as fold change relative to solvent control. Mean + SEM, $N = 3$, unpaired t-test, $^{*}P \leq 0.05$, ns = non-significant.

the RPS2-YFP reporter cells and the ENP1 readout (Figure 5B, Supplementary Figure S4A). Northern blot analysis of total RNA from DFMO-treated cells using a probe against the ITS2 region demonstrated an accumulation of the 32S pre-rRNA, indicating that ODC1 activity is required for 28S rRNA maturation (Figure 5D, E), consistent with the ODC1 depletion experiment. In contrast, rRNA processing intermediates of the 18S maturation pathway detected with the ITS1 probe were not changed significantly. In sum, two complementary approaches manipulating on the polyamine synthesis pathway, i.e. RNAi-mediated depletion of the rate-limiting enzymes AMD1 and ODC1 as well as DFMO-mediated inhibition of ODC1, confirmed the requirement of this pathway for ribosome biogenesis, and 60S subunit maturation in particular.

DISCUSSION

By performing two complementing genome-wide RNAi screens followed by a validation screen, we identified a function for at least 310 proteins in the maturation of the large ribosomal subunit in human cells. Most of these 310 high confidence screening hits fall into prominent functional protein clusters that comprise ribosomal proteins and RBFs, as expected, as well as key cellular modules such as chromatin organization and transcription, splicing, translation, and protein degradation, highlighting both the strong conservation of 60S subunit maturation from yeast to human and the interconnectivity of 60S synthesis with other fundamental cellular pathways. In addition, the hit list also contains many proteins that had previously not been implicated in ribosome biogenesis, including factors of unknown function. In the follow-up analysis, we concentrated on a cluster of proteins involved in polyamine synthesis. Depletion of the rate-limiting enzymes of the polyamine synthesis pathway AMD1 and ODC1, which both ranked high in the screen, as well as chemical inhibition of ODC1 activity with the small molecule inhibitor DFMO confirmed a critical role of this pathway in the synthesis of 60S subunits. Microscopy-based assays and pre-rRNA processing analysis revealed that nuclear steps of 60S subunit synthesis rely on polyamine

production. As a consequence, defects in polyamine synthesis lead to subunit imbalance and a shortage of 60S subunits.

To reduce the number of false-positives in our screening campaign, we not only used an average of seven siRNAs per gene but also applied very stringent thresholds for the generation of the final list of high confidence hits. As a consequence, the resulting hit list does not represent a complete inventory of factors required for 60S subunit synthesis, due to both our stringent cut-offs and the inherent nature of RNAi-based screens, which are known to suffer from false-negative results because of insufficient knockdown or hypomorphic effects (100). Therefore, several known 60S RBFs did not pass the chosen threshold criteria and were not defined as hits, including RRS1 (rank #710), BXDC1/RPF2 (rank #858) or LAS1L (rank #929). However, they still ranked in the top 5% of all tested genes. The appended full dataset containing hit rates of every tested siRNA (Supplementary Table S5) provides important information for researchers to judge the involvement of their genes-of-interest in 60S maturation. It is also important to point out that auxiliary, non-essential factors supporting ribosome biogenesis as well as quality control factors are likely not identified by our screening approach, since the used endpoint assay only captures strong effects on synthesis kinetics. Furthermore, the RPL29-GFP readout only allows to detect defects in nucleolar and nucleoplasmic steps of 60S maturation, while factors required for cytoplasmic maturation steps are likely not detected unless their depletion impairs the recycling of RBFs with a nuclear function. In conclusion, the use of stringent cut-offs enabled the generation of a high confidence list, while the full dataset provides further information on the potential involvement of other genes in the process.

As expected, the final hit list contained many *bona fide* RBFs and ribosomal proteins of both subunits as well as proteins of several other essential cellular modules such as factors involved in transcription, splicing, translation and cellular trafficking. Several hits in the cluster of transcription, mRNA processing and chromatin remodeling factors, including FOXN1, were unexpected. FOXN1 is an ortholog of yeast Fhl1, which binds to ribosomal protein gene promoters in yeast together with Esa1, Hmo1, Ifh1, Rap1 and Sfp1 (68,69,101,102). While regulation of ribosomal protein gene transcription is well understood in yeast, much less is known in the human system, where a common regulatory machinery for all ribosomal protein gene promoters seems to be lacking (69). Notably, a study investigating interactomes of transcription factors identified an interaction between FOXN1 and YY1, a transcription factor known to bind ribosomal protein gene promoters in human cells (103,104). Further, we identified KAT5, the human homolog of Esa1 in yeast, in the screen. KAT5 is part of the NuA4 complex and was previously shown to be recruited to ribosomal protein gene promoters in a MYC/MAX-dependent manner (105,106). Moreover, we found RUVBL1 and RUVBL2, which can associate via EP400 with the NuA4 complex, but also function as independent ATPases, e.g. in snoRNP synthesis (107,108). Overall, follow-up investigations of the function of FOXN1 and other factors in this cluster should shed more light on ribosomal protein gene regulation in human cells.

In another interesting cluster of hits, we identified components of the 26S proteasome as well as several E3 ligase components and the COP9 signalosome. The proteasome as well as several members of the ubiquitin proteasome system were also identified in a previous genome-wide screen for factors involved in 40S synthesis (30). Yet, even though proteasomal activity had been linked to ribosome maturation several years ago (109,110) little is known about the mechanistic contribution of the ubiquitin proteasome system to ribosome biogenesis in general and of the identified factors in particular. Our previous follow-up analysis of the 40S screen had confirmed a role of CRL4 and its constitutive E3 ligase components RBX1 and DDB1 in ribosome maturation (30). DDB1, RBX1 as well es the CRL4 substrate adaptors VPRBP and DCAF4L1, were also identified in this screen for 60S maturation factors, showing that CUL4 plays a role in both 40S and 60S synthesis. Notably, depletion of another E3 ubiquitin ligase, ZNRF3 also resulted in 60S biogenesis defects. ZNRF3 is an established negative regulator of the Wnt/β-catenin pathway (111). MYC and multiple 60S RBFs including the PeBoW complex have been previously identified as targets of Wnt/β-catenin signaling (112). Based on the diverse hits linked to the ubiquitin-proteasome system, we hypothesize that it influences ribosome maturation through several mechanisms.

An unexpected cluster of hits identified by our genome-wide screening approach was linked to polyamine metabolism. We validated these hits in follow-up experiments, revealing a strong dependency of 60S synthesis, including 28S and 5.8S rRNA processing, on polyamine synthesis. Polyamines function as modulators of various types of RNA by binding and stabilizing both single and double-stranded RNA in all kingdoms of life (77). Early studies in bacteria indicated that 12–15% of total polyamines are stably associated with ribosomes (86). Given their positive charge and stabilizing effect, we hypothesize that polyamines could be required as permanent structural components of 60S subunits and/or be necessary to chaperone rRNA folding during 60S biogenesis. Although direct evidence for such a model is hard to generate, this hypothesis is corroborated by several findings. Using a photoactivatable spermine analog in cross-linking experiments, spermine binding sites were mapped on the mature *E. coli* 16S (24 cross-links) and 23S (54 cross-links) rRNAs *in vitro* (113,114). In the large subunit, spermine binding sites clustered in functionally important regions including the PTC and tRNA binding sites. However, it is currently unclear, whether the mapped sites are bound by polyamines in a stable or transient manner (115,116).

In support of our hypothesis, polyamines have also been identified in several high-resolution electron density maps of ribosomal structures (117–119). One spermidine could be clearly mapped in a 2.4 Å structure of *E. coli* 70S ribosomes (117), and 17 polyamine moieties were found in a higher resolution 2.0 Å electron density map (119) (Supplementary Figure S5A). Most of these were localized

in the large 50S subunit, with a cluster of spermidines positioned close to the PTC and PET. Interestingly, when we overlayed the two cryo-EM structures, the location of the one spermidine found by Noeske and colleagues overlapped with the position of one of the 16 spermidines mapped in the structure by Watson and colleagues, indicating that this site is consistently bound by a spermidine molecule. In most high-resolution structures of eukaryotic ribosomes, polyamines have not been mapped, although two spermidine molecules were found close to the PET and PTC in a recent structure of a stalled mammalian ribosome solved at 2.8 Å (118), (Supplementary Figure S5B). However, when we aligned the bacterial 23S and mammalian 28S rRNA, it became apparent that the so far identified spermidine binding sites are located in different positions on the 60S subunit in bacteria and mammals. Most mapped 60S polyamine binding sites are buried deep in the core of the 60S subunit. While exchange of these polyamines is probably limited, some polyamines bound close to the PET are solvent-exposed and therefore likely exchangeable. As all these polyamine positions have been determined in structures obtained from ribosomes likely purified with polyamine-containing buffers, it remains to be clarified whether they can be confirmed in structures obtained from ribosomes that only encountered polyamines in living cells. Higher resolution electron density maps of human ribosomes will be key to faithfully map polyamine binding sites for analysis of their conservation. Together, cross-linking and high-resolution structures indicate that both spermidine and spermine are constitutive members of ribosomal subunits, which could explain the requirement of polyamine synthesis for ribosome maturation.

Currently, it is however unclear whether polyamines are directly involved in ribosomal subunit maturation as structural components of ribosomes as described above or if they support the process indirectly e.g. by their known contribution to translation (115). A direct influence of polyamines on translation efficiency was suggested by several studies, yet the precise mechanisms remain unclear. Notably, spermidine is also a co-substrate for EIF5A hypusination, a unique post-translational modification conserved in all eukaryotes (120). Hypusinated EIF5A supports peptide bond formation for difficult amino acid sequences such as polyprolines (121–123). EIF5A hypusination could thus influence ribosomal subunit maturation indirectly if EIF5A is required for translation of factors involved in ribosome biogenesis, such as ribosomal proteins or RBFs. Yet, depletion of deoxyhypusine synthase (DHPS) or deoxyhypusine hydrolase (DOHH), the two enzymes catalyzing EIF5A hypusination, did not result in 60S biogenesis defects in the screen. Because these are negative data, we cannot formally exclude an indirect effect of polyamine metabolism on ribosome biogenesis by translation. Nevertheless, we consider this as rather unlikely since we expect such a scenario to likely affect both 60S and 40S subunit maturation to the same extent. Given their molecular nature and their widespread function in cells, it will be challenging to decipher the role(s) of polyamines in ribosome maturation in detail, in particular in light of their contribution to the stability and function of mature ribosomes *in vitro* and *in vivo* (87,115,118). Several agents targeting polyamine synthesis and uptake are in clinical trials as combination therapies for cancer patients (124). Therefore, a better understanding of the role of polyamine metabolism in ribosome biogenesis, which is known to be closely linked to cancer progression, could further support the development of cancer treatment strategies.

In general, we expect that our screening dataset may serve as a rich resource for further research to better understand ribosome biogenesis and its regulation in human cells, which will be important to develop more specific therapeutic strategies for ribosomopathies and cancer.

DATA AVAILABILITY

Raw microscopy data of all screens are available in the ETH research collection (https://doi.org/10.3929/ethz-b-000528381).

SUPPLEMENTARY DATA

Supplementary Data are available at NAR Online.

ACKNOWLEDGEMENTS

We thank Dr I. Zemp and C. Ruggeri for critical reading of the manuscript, and the other members of the Kutay lab for helpful discussions. Microscopy and screening were performed on instruments of the ETHZ Microscopy Center (ScopeM). We thank M. Stebler and Dr G. Bodizs from ScopeM for technical support during screening.

FUNDING

Swiss National Science Foundation (SNSF) [31003A_166565 to U.K.]; NCCR 'RNA and disease'; R.H. and P.H. acknowledge support from the LENDULET-BIOMAG Grant [2018-342]; H2020-COMPASS-ERAPerMed; CZI Deep Visual Proteomics; H2020-DiscovAir; ELKH-Excellence grant. Funding for open access charge: snsf@chronoshub.io.
Conflict of interest statement. None declared.

REFERENCES

1. Klinge,S. and Woolford,J.L. (2019) Ribosome assembly coming into focus. *Nat. Rev. Mol. Cell Biol.*, **20**, 116–131.
2. Nerurkar,P., Altvater,M., Gerhardy,S., Schütz,S., Fischer,U., Weirich,C. and Panse,V.G. (2015) Eukaryotic ribosome assembly and nuclear export. *Int. Rev. Cell Mol. Biol.*, **319**, 107–140.
3. Peña,C., Hurt,E. and Panse,V.G. (2017) Eukaryotic ribosome assembly, transport and quality control. *Nature Publishing Group*, **24**, 689–699.
4. Woolford,J.L. and Baserga,S.J. (2013) Ribosome biogenesis in the yeast saccharomyces cerevisiae. *Genetics*, **195**, 643–681.
5. Zemp,I. and Kutay,U. (2007) Nuclear export and cytoplasmic maturation of ribosomal subunits. *FEBS Lett.*, **581**, 2783–2793.
6. Aubert,M., O'Donohue,M.-F., Lebaron,S. and Gleizes,P.-E. (2018) Pre-ribosomal RNA processing in human cells: from mechanisms to congenital diseases. *Biomolecules*, **8**, 123.
7. Henras,A.K., Plisson-Chastang,C., O'Donohue,M.-F., Chakraborty,A. and Gleizes,P.-E. (2015) An overview of pre-ribosomal RNA processing in eukaryotes. *WIREs RNA*, **6**, 225–242.

8. Bohnsack,K.E. and Bohnsack,M.T. (2019) Uncovering the assembly pathway of human ribosomes and its emerging links to disease. *EMBO J.*, **38**, e100278.
9. Tomecki,R., Sikorski,P.J. and Zakrzewska-Placzek,M. (2017) Comparison of preribosomal RNA processing pathways in yeast, plant and human cells – focus on coordinated action of endo- and exoribonucleases. *FEBS Lett.*, **591**, 1801–1850.
10. Kressler,D., Hurt,E. and Baßler,J. (2010) Driving ribosome assembly. *Biochim. Biophys. Acta - Mol. Cell Res.*, **1803**, 673–683.
11. Pelletier,J., Thomas,G. and Volarević,S. (2018) Ribosome biogenesis in cancer: new players and therapeutic avenues. *Nat. Rev. Cancer*, **18**, 51–63.
12. Warner,J.R. (1999) The economics of ribosome biosynthesis in yeast. *Trends Biochem. Sci*, **24**, 437–440.
13. Davide,R. (2012) Revisiting the nucleolus: from marker to dynamic integrator of cancer signaling. *Sci. Signal*, **5**, pe38.
14. Catez,F., Dalla Venezia,N., Marcel,V., Zorbas,C., Lafontaine,D.L.J. and Diaz,J.-J. (2019) Ribosome biogenesis: an emerging druggable pathway for cancer therapeutics. *Biochem. Pharmacol.*, **159**, 74–81.
15. Kampen,K.R., Sulima,S.O., Vereecke,S. and De Keersmaecker,K. (2020) Hallmarks of ribosomopathies. *Nucleic Acids Res.*, **48**, 1013–1028.
16. Farley-Barnes,K.I., Ogawa,L.M. and Baserga,S.J. (2019) Ribosomopathies: old concepts, new controversies. *Trends Genet.*, **35**, 754–767.
17. Donati,G., Peddigari,S., Mercer,C.A. and Thomas,G. (2013) 5S Ribosomal RNA is an essential component of a nascent ribosomal precursor complex that regulates the Hdm2-p53 checkpoint. *Cell Rep.*, **4**, 87–98.
18. Sloan,K.E., Bohnsack,M.T. and Watkins,N.J. (2013) The 5S RNP couples p53 homeostasis to ribosome biogenesis and nucleolar stress. *Cell Rep.*, **5**, 237–247.
19. Kressler,D., Hurt,E. and Baßler,J. (2017) A puzzle of life: crafting ribosomal subunits. *Trends Biochem. Sci*, **42**, 640–654.
20. Hurt,E., Hannus,S., Schmelzl,B., Lau,D., Tollervey,D. and Simos,G. (1999) A novel in vivo assay reveals inhibition of ribosomal nuclear export in ran-cycle and nucleoporin mutants. *J. Cell Biol.*, **144**, 389–401.
21. Stage-Zimmermann,T., Schmidt,U. and Silver,P.A. (2000) Factors affecting nuclear export of the 60S ribosomal subunit in vivo. *Mol. Biol. Cell*, **11**, 3777–3789.
22. Milkereit,P., Gadal,O., Podtelejnikov,A., Trumtel,S., Gas,N., Petfalski,E., Tollervey,D., Mann,M., Hurt,E. and Tschochner,H. (2001) Maturation and intranuclear transport of pre-ribosomes requires noc proteins. *Cell*, **105**, 499–509.
23. Baßler,J., Grandi,P., Gadal,O., Leßmann,T., Petfalski,E., Tollervey,D., Lechner,J. and Hurt,E. (2001) Identification of a 60S preribosomal particle that is closely linked to nuclear export. *Mol. Cell*, **8**, 517–529.
24. Grandi,P., Rybin,V., Baßler,J., Petfalski,E., Strauß,D., Marzioch,M., Schäfer,T., Kuster,B., Tschochner,H., Tollervey,D. *et al.* (2002) 90S pre-ribosomes include the 35S pre-rRNA, the U3 snoRNP, and 40S subunit processing factors but predominantly lack 60S synthesis factors. *Mol. Cell*, **10**, 105–115.
25. Nissan,T.A., Baßler,J., Petfalski,E., Tollervey,D. and Hurt,E. (2002) 60S pre-ribosome formation viewed from assembly in the nucleolus until export to the cytoplasm. *EMBO J.*, **21**, 5539–5547.
26. Fatica,A., Cronshaw,A.D., Dlaki,M. and Tollervey,D. (2002) Ssf1p prevents premature processing of an early pre-60S ribosomal particle. *Mol. Cell*, **9**, 341–351.
27. Dragon,F., Compagnone-Post,P.A., Mitchell,B.M., Porwancher,K.A., Wehner,K.A., Wormsley,S., Settlage,R.E., Shabanowitz,J., Osheim,Y., Beyer,A.L. *et al.* (2002) A large nucleolar U3 ribonucleoprotein required for 18S ribosomal RNA biogenesis. *Nature*, **417**, 967–970.
28. Schäfer,T., Strauß,D., Petfalski,E., Tollervey,D. and Hurt,E. (2003) The path from nucleolar 90S to cytoplasmic 40S pre-ribosomes. *EMBO J.*, **22**, 1370–1380.
29. Farley-Barnes,K.I., McCann,K.L., Ogawa,L.M., Merkel,J., Surovtseva,Y. v. and Baserga,S.J. (2018) Diverse regulators of human ribosome biogenesis discovered by changes in nucleolar number. *Cell Rep.*, **22**, 1923–1934.
30. Badertscher,L., Wild,T., Montellese,C., Alexander,L.T., Bammert,L., Sarazova,M., Stebler,M., Csucs,G., Mayer,T.U., Zamboni,N. *et al.* (2015) Genome-wide RNAi screening identifies protein modules required for 40S subunit synthesis in human cells. *Cell Rep.*, **13**, 2879–2891.
31. Wild,T., Horvath,P., Wyler,E., Widmann,B., Badertscher,L., Zemp,I., Kozak,K., Csucs,G., Lund,E. and Kutay,U. (2010) A protein inventory of human ribosome biogenesis reveals an essential function of exportin 5 in 60S subunit export. *PLoS Biol.*, **8**, e1000522.
32. Tafforeau,L., Zorbas,C., Langhendries,J.L., Mullineux,S.T., Stamatopoulou,V., Mullier,R., Wacheul,L. and Lafontaine,D.L.J. (2013) The complexity of human ribosome biogenesis revealed by systematic nucleolar screening of pre-rRNA processing factors. *Mol. Cell*, **51**, 539–551.
33. Ogawa,L.M., Buhagiar,A.F., Abriola,L., Leland,B.A., Surovtseva,Y. v. and Baserga,S.J. (2021) Increased numbers of nucleoli in a genome-wide RNAi screen reveal proteins that link the cell cycle to RNA polymerase I transcription. *Mol. Biol. Cell*, **32**, 956–973.
34. Wyler,E., Zimmermann,M., Widmann,B., Gstaiger,M., Pfannstiel,J., Kutay,U. and Zemp,I. (2011) Tandem affinity purification combined with inducible shRNA expression as a tool to study the maturation of macromolecular assemblies. *RNA*, **17**, 189–200.
35. Zemp,I., Wild,T., O'Donohue,M.F., Wandrey,F., Widmann,B., Gleizes,P.E. and Kutay,U. (2009) Distinct cytoplasmic maturation steps of 40S ribosomal subunit precursors require hRio2. *J. Cell Biol.*, **185**, 1167–1180.
36. Wyler,E., Wandrey,F., Badertscher,L., Montellese,C., Alper,D. and Kutay,U. (2014) The beta-isoform of the BRCA2 and CDKN1A(p21)-interacting protein (BCCIP) stabilizes nuclear RPL23/uL14. *FEBS Lett.*, **588**, 3685–3691.
37. Smith,K., Li,Y., Piccinini,F., Csucs,G., Balazs,C., Bevilacqua,A. and Horvath,P. (2015) CIDRE: an illumination-correction method for optical microscopy. *Nat. Methods*, **12**, 404–406.
38. Carpenter,A.E., Jones,T.R., Lamprecht,M.R., Clarke,C., Kang,I.H., Friman,O., Guertin,D.A., Chang,J.H., Lindquist,R.A., Moffat,J. *et al.* (2006) CellProfiler: image analysis software for identifying and quantifying cell phenotypes. *Genome Biol.*, **7**, R100.
39. Hollandi,R., Szkalisity,A., Toth,T., Tasnadi,E., Molnar,C., Mathe,B., Grexa,I., Molnar,J., Balind,A., Gorbe,M. *et al.* (2020) nucleAIzer: a parameter-free deep learning framework for nucleus segmentation using image style transfer. *Cell Syst.*, **10**, 453–458.
40. Piccinini,F., Balassa,T., Szkalisity,A., Molnar,C., Paavolainen,L., Kujala,K., Buzas,K., Sarazova,M., Pietiainen,V., Kutay,U. *et al.* (2017) Advanced cell classifier: user-friendly machine-learning-based software for discovering phenotypes in high-content imaging data. *Cell Syst.*, **4**, 651–655.
41. König,R., Chiang,C., Tu,B.P., Yan,S.F., DeJesus,P.D., Romero,A., Bergauer,T., Orth,A., Krueger,U., Zhou,Y. *et al.* (2007) A probability-based approach for the analysis of large-scale RNAi screens. *Nat. Methods*, **4**, 847–849.
42. Szklarczyk,D., Gable,A.L., Lyon,D., Junge,A., Wyder,S., Huerta-Cepas,J., Simonovic,M., Doncheva,N.T., Morris,J.H., Bork,P. *et al.* (2019) STRING v11: protein–protein association networks with increased coverage, supporting functional discovery in genome-wide experimental datasets. *Nucleic Acids Res.*, **47**, D607–D613.
43. Shannon,P., Markiel,A., Ozier,O., Baliga,N.S., Wang,J.T., Ramage,D., Amin,N., Schwikowski,B. and Ideker,T. (2003) Cytoscape: a software environment for integrated models of biomolecular interaction networks. *Genome Res.*, **13**, 2498–2504.
44. Mi,H., Ebert,D., Muruganujan,A., Mills,C., Albou,L.-P., Mushayamaha,T. and Thomas,P.D. (2021) PANTHER version 16: a revised family classification, tree-based classification tool, enhancer regions and extensive API. *Nucleic Acids Res.*, **49**, D394–D403.
45. Piñero,J., Ramírez-Anguita,J.M., Saüch-Pitarch,J., Ronzano,F., Centeno,E., Sanz,F. and Furlong,L.I. (2020) The DisGeNET knowledge platform for disease genomics: 2019 update. *Nucleic Acids Res.*, **48**, D845–D855.
46. Rouquette,J., Choesmel,V. and Gleizes,P.E. (2005) Nuclear export and cytoplasmic processing of precursors to the 40S ribosomal subunits in mammalian cells. *EMBO J.*, **24**, 2862–2872.
47. Thomas,F. and Kutay,U. (2003) Biogenesis and nuclear export of ribosomal subunits in higher eukaryotes depend on the CRM1 export pathway. *J. Cell Sci.*, **116**, 2409–2419.

48. Trotta,C.R., Lund,E., Kahan,L., Johnson,A.W. and Dahlberg,J.E. (2003) Coordinated nuclear export of 60s ribosomal subunits and NMD3 in vertebrates. *EMBO J.*, **22**, 2841–2851.
49. Weil,D., Garçon,L., Harper,M., Duménil,D., Dautry,F. and Kress,M. (2002) Targeting the kinesin Eg5 to monitor siRNA transfection in mammalian cells. *BioTechniques*, **33**, 1244–1248.
50. Louise,von S., Dimitris,T., Jordi,C.P., Laurens,O., Ramakrishnaiah,S., Alex,P., Harry,V., Bob,van de W., Leon,H.F. and Erik,H.J.D. (2015) The E3 ubiquitin ligase ARIH1 protects against genotoxic stress by initiating a 4EHP-Mediated mRNA translation arrest. *Mol. Cell. Biol.*, **35**, 1254–1268.
51. Zanin,E., Desai,A., Poser,I., Toyoda,Y., Andree,C., Moebius,C., Bickle,M., Conradt,B., Piekny,A. and Oegema,K. (2013) A conserved RhoGAP limits m phase contractility and coordinates with microtubule asters to confine RhoA during cytokinesis. *Dev. Cell*, **26**, 496–510.
52. Nagaraj,N., Wisniewski,J.R., Geiger,T., Cox,J., Kircher,M., Kelso,J., Pääbo,S. and Mann,M. (2011) Deep proteome and transcriptome mapping of a human cancer cell line. *Mol. Syst. Biol.*, **7**, 548.
53. Schaab,C., Geiger,T., Stoehr,G., Cox,J. and Mann,M. (2012) Analysis of high accuracy, quantitative proteomics data in the MaxQB database. *Mol. Cell. Proteomics*, **11**, M111.014068.
54. Hannus,M., Beitzinger,M., Engelmann,J.C., Weickert,M.-T., Spang,R., Hannus,S. and Meister,G. (2014) siPools: highly complex but accurately defined siRNA pools eliminate off-target effects. *Nucleic Acids Res.*, **42**, 8049–8061.
55. Thul,P.J., Åkesson,L., Wiking,M., Mahdessian,D., Geladaki,A., Ait Blal,H., Alm,T., Asplund,A., Björk,L., Breckels,L.M. *et al.* (2017) A subcellular map of the human proteome. *Science*, **356**, eaal3321.
56. Ahmad,Y., Boisvert,F.-M., Gregor,P., Cobley,A. and Lamond,A.I. (2009) NOPdb: nucleolar proteome database-2008 update. *Nucleic Acids Res.*, **37**, D181–D184.
57. Leung,A.K.L., Trinkle-Mulcahy,L., Lam,Y.W., Andersen,J.S., Mann,M. and Lamond,A.I. (2006) NOPdb: nucleolar proteome database. *Nucleic Acids Res.*, **34**, D218–D220.
58. Andersen,J.S., Lam,Y.W., Leung,A.K.L., Ong,S.-E., Lyon,C.E., Lamond,A.I. and Mann,M. (2005) Nucleolar proteome dynamics. *Nature*, **433**, 77–83.
59. Ashburner,M., Ball,C.A., Blake,J.A., Botstein,D., Butler,H., Cherry,J.M., Davis,A.P., Dolinski,K., Dwight,S.S., Eppig,J.T. *et al.* (2000) Gene ontology: tool for the unification of biology. *Nat. Genet.*, **25**, 25–29.
60. Rocak,S., Emery,B., Tanner,N.K. and Linder,P. (2005) Characterization of the ATPase and unwinding activities of the yeast DEAD-box protein has1p and the analysis of the roles of the conserved motifs. *Nucleic Acids Res.*, **33**, 999–1009.
61. Cosmin,S., Abdelkader,N., Pierre-Emmanuel,G., Alice,L., Jean-Claude,R., Jacqueline,N.-D., Nicole,G., Alain,J. and Micheline,F.-R. (2003) Sequential protein association with nascent 60S ribosomal particles. *Mol. Cell. Biol.*, **23**, 4449–4460.
62. Prieto,J.-L. and McStay,B. (2007) Recruitment of factors linking transcription and processing of pre-rRNA to NOR chromatin is UBF-dependent and occurs independent of transcription in human cells. *Genes Dev.*, **21**, 2041–2054.
63. Gallagher,J.E.G., Dunbar,D.A., Granneman,S., Mitchell,B.M., Osheim,Y., Beyer,A.L. and Baserga,S.J. (2004) RNA polymerase i transcription and pre-rRNA processing are linked by specific SSU processome components. *Genes Dev.*, **18**, 2506–2517.
64. Zhang,Y., Forys,J.T., Miceli,A.P., Gwinn,A.S. and Weber,J.D. (2011) Identification of DHX33 as a mediator of rRNA synthesis and cell growth. *Mol. Cell. Biol.*, **31**, 4676–4691.
65. Valdez,B.C., Henning,D., So,R.B., Dixon,J. and Dixon,M.J. (2004) The treacher collins syndrome TCOF1 gene product is involved in ribosomal DNA gene transcription by interacting with upstream binding factor. *Proc. Nat. Acad. Sci. U.S.A.*, **101**, 10709.
66. Ishiguro,A., Kassavetis,G.A. and Geiduschek,E.P. (2002) Essential roles of bdp1, a subunit of RNA polymerase III initiation factor TFIIIB, in transcription and tRNA processing. *Mol. Cell. Biol.*, **22**, 3264–3275.
67. van Riggelen,J., Yetil,A. and Felsher,D.W. (2010) MYC as a regulator of ribosome biogenesis and protein synthesis. *Nat. Rev. Cancer*, **10**, 301–309.
68. Rudra,D., Zhao,Y. and Warner,J.R. (2005) Central role of ifh1p–fhl1p interaction in the synthesis of yeast ribosomal proteins. *EMBO J.*, **24**, 533–542.
69. Petibon,C., Malik Ghulam,M., Catala,M. and Abou Elela,S. (2021) Regulation of ribosomal protein genes: an ordered anarchy. *WIREs RNA*, **12**, e1632.
70. Clarke,A.S., Lowell,J.E., Jacobson,S.J. and Pillus,L. (1999) Esa1p is an essential histone acetyltransferase required for cell cycle progression. *Mol. Cell. Biol.*, **19**, 2515–2526.
71. Cai,Y., Jin,J., Tomomori-Sato,C., Sato,S., Sorokina,I., Parmely,T.J., Conaway,R.C. and Conaway,J.W. (2003) Identification of new subunits of the multiprotein mammalian TRRAP/TIP60-containing histone acetyltransferase complex*. *J. Biol. Chem.*, **278**, 42733–42736.
72. Schuettengruber,B., Martinez,A.-M., Iovino,N. and Cavalli,G. (2011) Trithorax group proteins: switching genes on and keeping them active. *Nat. Rev. Mol. Cell Biol.*, **12**, 799–814.
73. Wu,M., Peng,F.W., Lee,J.S., Martin-Brown,S., Florens,L., Washburn,M. and Shilatifard,A. (2008) Molecular regulation of H3K4 trimethylation by wdr82, a component of human Set1/COMPASS. *Mol. Cell. Biol.*, **28**, 7337–7344.
74. Ceulemans,H. and Bollen,M. (2004) Functional diversity of protein phosphatase-1, a cellular economizer and reset button. *Physiol. Rev.*, **84**, 1–39.
75. Chamousset,D., De Wever,V., Moorhead,G.B., Chen,Y., Boisvert,F.-M., Lamond,A.I. and Trinkle-Mulcahy,L. (2010) RRP1B targets PP1 to mammalian cell nucleoli and is associated with Pre-60S ribosomal subunits. *Mol. Biol. Cell*, **21**, 4212–4226.
76. Han,X.-R., Sasaki,N., Jackson,S.C., Wang,P., Li,Z., Smith Matthew,D, Xie,L., Chen,X., Zhang,Y., Marzluff,W.F. *et al.* (2021) CRL4DCAF1/VprBP E3 ubiquitin ligase controls ribosome biogenesis, cell proliferation, and development. *Sci. Adv.*, **6**, eabd6078.
77. Lightfoot,H.L. and Hall,J. (2014) Endogenous polyamine function—the RNA perspective. *Nucleic Acids Res.*, **42**, 11275–11290.
78. Bae,D.-H., Lane,D.J.R., Jansson,P.J. and Richardson,D.R. (2018) The old and new biochemistry of polyamines. *Biochim. Biophys. Acta (BBA) - Gen. Subj.*, **1862**, 2053–2068.
79. Tabor,C.W. and Tabor,H. (1984) Polyamines. *Annu. Rev. Biochem.*, **53**, 749–790.
80. Pegg,A.E., Lockwood,D.H. and Williams-Ashman,H.G. (1970) Concentrations of putrescine and polyamines and their enzymic synthesis during androgen-induced prostatic growth. *Biochem. J.*, **117**, 17–31.
81. Murakami,Y., Matsufuji,S., Kameji,T., Hayashi,S., Igarashi,K., Tamura,T., Tanaka,K. and Ichihara,A. (1992) Ornithine decarboxylase is degraded by the 26S proteasome without ubiquitination. *Nature*, **360**, 597–599.
82. Murakami,Y., Ichiba,T., Matsufuji,S. and Hayashi,S. (1996) Cloning of antizyme inhibitor, a highly homologous protein to ornithine decarboxylase. *J. Biol. Chem.*, **271**, 3340–3342.
83. López-Contreras,A.J., López-Garcia,C., Jiménez-Cervantes,C., Cremades,A. and Peñafiel,R. (2006) Mouse ornithine Decarboxylase-like gene encodes an antizyme inhibitor devoid of ornithine and arginine decarboxylating activity. *J. Biol. Chem.*, **281**, 30896–30906.
84. Mangold,U. and Leberer,E. (2004) Regulation of all members of the antizyme family by antizyme inhibitor. *Biochem. J.*, **385**, 21–28.
85. Agrawal,R.K., Penczek,P., Grassucci,R.A., Burkhardt,N., Nierhaus,K.H. and Frank,J. (1999) Effect of buffer conditions on the position of tRNA on the 70 s ribosome as visualized by cryoelectron microscopy. *J. Biol. Chem.*, **274**, 8723–8729.
86. Cohen,S.S. and Lichtenstein,J. (1960) Polyamines and ribosome structure. *J. Biol. Chem.*, **235**, 2112–2116.
87. Atkins,J.F., Lewis,J.B., Anderson,C.W. and Gesteland,R.F. (1975) Enhanced differential synthesis of proteins in a mammalian cell-free system by addition of polyamines. *J. Biol. Chem.*, **250**, 5688–5695.
88. Siekevitz,P. and Palade,G.E. (1962) Cytochemical study on the pancreas of the guinea pig: VII. Effects of spermine on ribosomes. *J. Cell Biol.*, **13**, 217–232.
89. Hölttä,E. and Hovi,T. (1985) Polyamine depletion results in impairment of polyribosome formation and protein synthesis before

onset of DNA synthesis in mitogen-activated human lymphocytes. *Eur. J. Biochem.*, **152**, 229–237.
90. Kashiwagi,K., Sakai,Y. and Igarashi,K. (1989) Polyamine stimulation of ribosomal synthesis and activity in a polyamine-dependent mutant of escherichia coli. *Arch. Biochem. Biophys.*, **268**, 379–387.
91. Bernstein,K.A., Gallagher,J.E.G., Mitchell,B.M., Granneman,S. and Baserga,S.J. (2004) The small-subunit processome is a ribosome assembly intermediate. *Eukaryot. Cell.*, **3**, 1619–1626.
92. Chen,W., Bucaria,J., Band,D.A., Sutton,A. and Sternglanz,R. (2003) Enp1, a yeast protein associated with U3 and U14 snoRNAs, is required for pre-rRNA processing and 40S subunit synthesis. *Nucleic Acids Res.*, **31**, 690–699.
93. Oeffinger,M., Dlakić,M. and Tollervey,D. (2004) A pre-ribosome-associated HEAT-repeat protein is required for export of both ribosomal subunits. *Genes Dev.*, **18**, 196–209.
94. Metcalf,B.W., Bey,P., Danzin,C., Jung,M.J., Casara,P. and Vevert,J.P. (1978) Catalytic irreversible inhibition of mammalian ornithine decarboxylase (E.C.4.1.1.17) by substrate and product analogs. *J. Am. Chem. Soc.*, **100**, 2551–2553.
95. Poulin,R., Lu,L., Ackermann,B., Bey,P. and Pegg,A.E. (1992) Mechanism of the irreversible inactivation of mouse ornithine decarboxylase by alpha-difluoromethylornithine. Characterization of sequences at the inhibitor and coenzyme binding sites. *J. Biol. Chem.*, **267**, 150–158.
96. Kramer,D.L., Chang,B.-D., Chen,Y., Diegelman,P., Alm,K., Black,A.R., Roninson,I.B. and Porter,C.W. (2001) Polyamine depletion in human melanoma cells leads to G_1 arrest associated with induction of $p21^{WAF1/CIP1/SDI1}$, changes in the expression of p21-regulated genes, and a Senescence-like phenotype. *Cancer Res.*, **61**, 7754.
97. Ray,R.M., Bhattacharya,S., Bavaria,M.N., Viar,M.J. and Johnson,L.R. (2014) Antizyme (AZ) regulates intestinal cell growth independent of polyamines. *Amino Acids*, **46**, 2231–2239.
98. Gerner,E.W. and Mamont,P.S. (1986) Restoration of the polyamine contents in rat hepatoma tissue-culture cells after inhibition of polyamine biosynthesis. *Eur. J. Biochem.*, **156**, 31–35.
99. Landau,G., Ran,A., Bercovich,Z., Feldmesser,E., Horn-Saban,S., Korkotian,E., Jacob-Hirsh,J., Rechavi,G., Ron,D. and Kahana,C. (2012) Expression profiling and biochemical analysis suggest stress response as a potential mechanism inhibiting proliferation of Polyamine-depleted cells. *J. Biol. Chem.*, **287**, 35825–35837.
100. Housden,B.E. and Perrimon,N. (2016) Comparing CRISPR and RNAi-based screening technologies. *Nat. Biotechnol.*, **34**, 621–623.
101. Wade,J.T., Hall,D.B. and Struhl,K. (2004) The transcription factor ifh1 is a key regulator of yeast ribosomal protein genes. *Nature*, **432**, 1054–1058.
102. Zhao,Y., McIntosh,K.B., Rudra,D., Schawalder,S., Shore,D. and Warner,J.R. (2006) Fine-structure analysis of ribosomal protein gene transcription. *Mol. Cell. Biol.*, **26**, 4853–4862.
103. Li,X., Wang,W., Wang,J., Malovannaya,A., Xi,Y., Li,W., Guerra,R., Hawke,D.H., Qin,J. and Chen,J. (2015) Proteomic analyses reveal distinct chromatin-associated and soluble transcription factor complexes. *Mol. Syst. Biol.*, **11**, 775.
104. Chen,L., Shioda,T., Coser,K.R., Lynch,M.C., Yang,C. and Schmidt,E. v (2010) Genome-wide analysis of YY2 versus YY1 target genes. *Nucleic Acids Res.*, **38**, 4011–4026.
105. Frank,S.R., Schroeder,M., Fernandez,P., Taubert,S. and Amati,B. (2001) Binding of c-Myc to chromatin mediates mitogen-induced acetylation of histone H4 and gene activation. *Genes Dev.*, **15**, 2069–2082.
106. Bouchard,C., Dittrich,O., Kiermaier,A., Dohmann,K., Menkel,A., Eilers,M. and Lüscher,B. (2001) Regulation of cyclin D2 gene expression by the myc/max/mad network: Myc-dependent TRRAP recruitment and histone acetylation at the cyclin D2 promoter. *Genes Dev.*, **15**, 2042–2047.
107. Boulon,S., Marmier-Gourrier,N., Pradet-Balade,B., Wurth,L., Verheggen,C., Jády,B.E., Rothé,B., Pescia,C., Robert,M.-C., Kiss,T. *et al.* (2008) The hsp90 chaperone controls the biogenesis of L7Ae RNPs through conserved machinery. *J. Cell Biol.*, **180**, 579–595.
108. Cloutier,P., Poitras,C., Durand,M., Hekmat,O., Fiola-Masson,É., Bouchard,A., Faubert,D., Chabot,B. and Coulombe,B. (2017) R2TP/Prefoldin-like component RUVBL1/RUVBL2 directly interacts with ZNHIT2 to regulate assembly of U5 small nuclear ribonucleoprotein. *Nat. Commun.*, **8**, 15615.
109. Fátyol,K. and Grummt,I. (2008) Proteasomal ATPases are associated with rDNA: the ubiquitin proteasome system plays a direct role in RNA polymerase i transcription. *Biochim. Biophys. Acta (BBA) - Gene Regul. Mech.*, **1779**, 850–859.
110. Stavreva,D.A., Kawasaki,M., Dundr,M., Koberna,K., Müller,W.G., Tsujimura-Takahashi,T., Komatsu,W., Hayano,T., Isobe,T., Raska,I. *et al.* (2006) Potential roles for ubiquitin and the proteasome during ribosome biogenesis. *Mol. Cell. Biol.*, **26**, 5131–5145.
111. Hao,H.-X., Xie,Y., Zhang,Y., Charlat,O., Oster,E., Avello,M., Lei,H., Mickanin,C., Liu,D., Ruffner,H. *et al.* (2012) ZNRF3 promotes wnt receptor turnover in an R-spondin-sensitive manner. *Nature*, **485**, 195–200.
112. Pfister,A.S. and Kühl,M. (2018) Chapter four - Of Wnts and ribosomes. In: Larraín,J. and Olivares,G.B.T-.P. (eds). *WNT Signaling in Health and Disease*. Academic Press, Vol. **153**, pp. 131–155.
113. Amarantos,I., Zarkadis,I.K. and Kalpaxis,D.L. (2002) The identification of spermine binding sites in 16S rRNA allows interpretation of the spermine effect on ribosomal 30S subunit functions. *Nucleic Acids Res.*, **30**, 2832–2843.
114. Xaplanteri,M.A., Petropoulos,A.D., Dinos,G.P. and Kalpaxis,D.L. (2005) Localization of spermine binding sites in 23S rRNA by photoaffinity labeling: parsing the spermine contribution to ribosomal 50S subunit functions. *Nucleic Acids Res.*, **33**, 2792–2805.
115. Dever,T.E. and Ivanov,I.P. (2018) Roles of polyamines in translation. *J. Biol. Chem.*, **293**, 18719–18729.
116. Rozov,A., Khusainov,I., El Omari,K., Duman,R., Mykhaylyk,V., Yusupov,M., Westhof,E., Wagner,A. and Yusupova,G. (2019) Importance of potassium ions for ribosome structure and function revealed by long-wavelength X-ray diffraction. *Nat. Commun.*, **10**, 2519.
117. Noeske,J., Wasserman,M.R., Terry,D.S., Altman,R.B., Blanchard,S.C. and Cate,J.H.D. (2015) High-resolution structure of the *Escherichia coli* ribosome. *Nat. Struct. Mol. Biol.*, **22**, 336–341.
118. Chandrasekaran,V., Juszkiewicz,S., Choi,J., Puglisi,J.D., Brown,A., Shao,S., Ramakrishnan,V. and Hegde,R.S. (2019) Mechanism of ribosome stalling during translation of a poly(A) tail. *Nat. Struct. Mol. Biol.*, **26**, 1132–1140.
119. Watson,Z.L., Ward,F.R., Méheust,R., Ad,O., Schepartz,A., Banfield,J.F. and Cate,J.H.D. (2020) Structure of the bacterial ribosome at 2 Å resolution. *eLife*, **9**, e60482.
120. Park,M.H. and Wolff,E.C. (2018) Hypusine, a polyamine-derived amino acid critical for eukaryotic translation. *J. Biol. Chem.*, **293**, 18710–18718.
121. Pelechano,V. and Alepuz,P. (2017) eIF5A facilitates translation termination globally and promotes the elongation of many non polyproline-specific tripeptide sequences. *Nucleic Acids Res.*, **45**, 7326–7338.
122. Gutierrez,E., Shin,B.-S., Woolstenhulme,C.J., Kim,J.-R., Saini,P., Buskirk,A.R. and Dever,T.E. (2013) eIF5A promotes translation of polyproline motifs. *Mol. Cell*, **51**, 35–45.
123. Shin,B.-S., Katoh,T., Gutierrez,E., Kim,J.-R., Suga,H. and Dever,T.E. (2017) Amino acid substrates impose polyamine, eIF5A, or hypusine requirement for peptide synthesis. *Nucleic Acids Res.*, **45**, 8392–8402.
124. Casero,R.A., Murray Stewart,T. and Pegg,A.E. (2018) Polyamine metabolism and cancer: treatments, challenges and opportunities. *Nat. Rev. Cancer*, **18**, 681–695.